Ground motion simulations of a major historical earthquake (1660) in the French Pyrenees using recent moderate size earthquakes

L. Honoré, F. Courboulex, A. Souriau,

Geophysical Journal International

Geophys. J. Int. (2011) **187,** 1001–1018 doi: 10.1111/j.1365-246X.2011.05193.x

Ground motion simulations of a major historical earthquake (1660) in the French Pyrenees using recent moderate size earthquakes

Laëtitia Honoré,[1] Françoise Courboulex[1] and Annie Souriau[2]

[1] *Université de Nice Sophia-Antipolis, CNRS, Géoazur, Observatoire de la Côte d'Azur, Valbonne, France. E-mail: honorel@geoazur.unice.fr*
[2] *CNRS, Université Paul Sabatier, Observatoire Midi-Pyrénées, Toulouse, France*

Accepted 2011 August 16. Received 2011 June 5; in original form 2010 September 21

SUMMARY

In regions where only small- to moderate-size events have been recorded, it is important to be able to anticipate the effects of a large event by simulating the ground motion it may generate. Using the very good records of two small earthquakes that occurred in the central French Pyrenees (2007 November 15, $M_w = 3.6$; and 2006 November 17, $M_w = 4.5$), we simulated the ground motions generated by a magnitude 6.1 earthquake, equivalent to a historical event that struck the region in 1660. This major earthquake caused severe damage and reached a maximum macroseismic intensity of IX on the MSK scale. The simulation is based on the empirical Green's function (EGF) method, which allows simulations in a broad frequency range, and accounts for both propagation and site effects. We first validated the method by reproducing the records of the $M_w = 4.5$ earthquake using the $M_w = 3.6$ earthquake as an EGF. A careful analysis of corner frequencies and spectral ratios revealed a clear directivity effect of the rupture process for the larger event ($M_w = 4.5$). When this directivity is taken into account in the simulation, a very good reproduction of the $M_w = 4.5$ ground motion parameters is obtained at all the stations. We then used the records of the $M_w = 3.6$ earthquake as an EGF for simulating the historical event. At 11 stations we computed a large number of synthetic accelerograms that aim to account for the possible source variability of an $M_w = 6.1$ earthquake. The comparison between the computed ground accelerations and those given by three different empirical ground motion prediction equations (GMPEs) reveals that simulation is quite successful. Finally, our simulation results are compared with intensity data of the 1660 event, by use of three different Ground Motion Intensity Conversion Equations (GMICEs). We found that the intensity levels predicted from ground motion simulations are systematically lower than the reported macroseismic intensities. To explain this difference, the hypothesis of a possible underestimation of the magnitude of the 1660 event is discussed.

Key words Earthquake ground motions; Earthquake source observations; Seismicity and tectonics; Site effects; Computational seismology; Europe.

1 INTRODUCTION

The Pyrenean range is characterized by moderate seismic activity. Since the systematic deployment of seismic networks in the early sixties, the largest recorded event reached a magnitude of $M_l = 5.5$ (1967 August 13 Arette earthquake, Gagnepain *et al.* 1980). However, several strong earthquakes with epicentral intensity larger than VIII have been reported in historical catalogues (Lambert & Levret-Albaret 1996). One of the most destructive Pyrenean earthquakes occurred in the Central French Pyrenees, on 1660 June 21. Based on reported damage, the suspected epicentral region is located a few kilometres south of the pilgrimage city of Lourdes, and its epicentral intensity is assessed at VIII–IX on the MSK scale (1964) (SisFrance, BRGM *et al.* 2004). Its magnitude is estimated to be equivalent to 6.1 (Levret *et al.* 1996).

If a similar earthquake were to occur today, it would likely induce major destruction and casualties because of the urban development and the increased population in the Lourdes region. Thus, it is of major importance to better anticipate a hypothetical future large earthquake by providing information of engineering interest. The quantification of the ground motions generated by the large historical earthquakes is therefore of major interest.

There are essentially three kinds of approach to estimate the ground motions generated by an earthquake:

(1) Empirical ground motion prediction equations (GMPEs): These equations provide ground motion parameters as a function of magnitude, source-to-site distance and other variables such as local soil conditions or style of faulting (e.g. Reiter 1990; Douglas 2003). These relations are empirically derived through regression analysis

from the recorded ground motion database. To establish GMPEs, data from a broad range of magnitudes and source-to-site distances are necessary. In regions of low to moderate seismicity, there are not enough ground motion records to develop a specific GMPE. Data recorded in other regions in the world have to be used, assuming that they are appropriate for the area concerned. GMPEs are essential for seismic hazard assessment, but they are neither able to provide accelerograms, nor to reproduce specific attenuation conditions and site effects.

(2) Numerical methods: They are based on modelling of both source process and seismic wave propagation in a heterogeneous medium. These methods are promising; however, they are often limited to rather low frequencies due to the poor knowledge of structure velocities, and to unknown details of the rupture process of the event.

(3) Semi-empirical approaches: They are often based on the empirical Green's function (EGF) principle (Hartzell 1978). The basic idea is to consider records of a small earthquake, located near an event of interest, as a reasonable approximation of the impulse response of the medium. This approach allows us to simulate seismograms of a large earthquake that account for wave-propagation and site-effects, under the assumption of linear soil response. However, as in (2), the rupture history is generally unknown.

The goal of this study is to produce ground motion simulations of a magnitude $M_w = 6.1$ earthquake, equivalent to the 1660 historical event, from instrumental data of recent small to moderate Pyrenean earthquakes. To do so, we propose to use the method developed by Kohrs-Sansorny *et al.* (2005), where ground motion simulations of a large earthquake are generated by using a stochastic summation of the records of a small earthquake, regarded as EGFs. This method is easy to implement and has the advantage of requiring very few input parameters, as the stochastic approach compensates for the poor knowledge of the source characteristics.

On 2006 November 17 and 2007 November 15, two Pyrenean earthquakes (respectively $M_w = 4.5$ and $M_w = 3.6$) occurred in the suspected epicentral area of the 1660 historical event. They were well recorded by a large number of accelerometric stations (French Permanent Accelerometric Network, Pequegnat *et al*. 2008), thus providing us with the opportunity to implement an EGF simulation method (Fig. 1).

In a first step, we used the 2007 earthquake ($M_w = 3.6$) as an EGF to reproduce ground motions generated by the 2006 earthquake ($M_w = 4.5$). The direct comparison between simulation results and ground motions observed during the 2006 earthquake allowed us to evaluate the efficiency and limitations of the method.

In a second step, we aimed to generate ground motion simulations of a magnitude $M_w = 6.1$ earthquake, by using the 2007 earthquake ($M_w = 3.6$) as an EGF. These simulations provided us with estimations of ground motions that could realistically be generated at specific Pyrenean stations by an earthquake equivalent to the 1660 historical event. To compare our simulation results with the intensity data of the 1660 event, empirical relationships between instrumental ground motion parameters and macroseismic intensities (GMICEs) have been used.

2 SEISMOTECTONIC CONTEXT

2.1 Tectonic setting and seismicity

The Pyrenean range results from the Cenozoic north–south convergence of the Eurasian Plate and the Iberian microplate, initiated 65

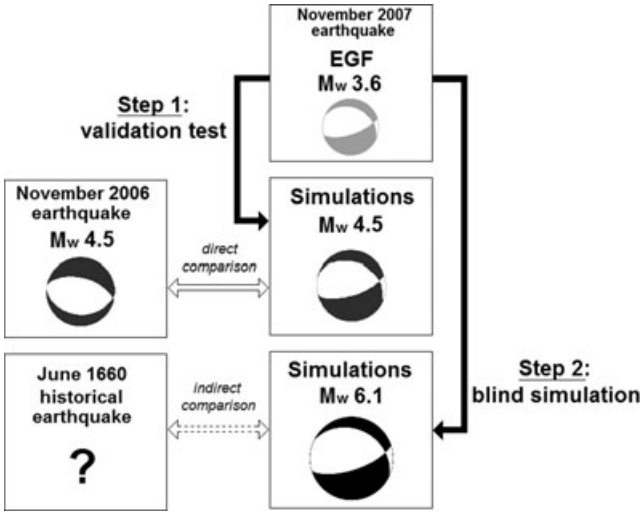

Figure 1. The two principal steps of the study. In Step 1 (validation test) the 2007 earthquake ($M_w = 3.6$) is used as an empirical Green's function to reproduce ground motions generated by the 2006 earthquake ($M_w = 4.5$). Simulation results and ground motions observed during the 2006 earthquake are directly compared. In Step 2 (blind simulation) the 2007 earthquake ($M_w = 3.6$) is used as an empirical Green's function to produce ground motion simulations of a magnitude $M_w = 6.1$ earthquake, equivalent to the 1660 historical event. Simulation results and intensity data of the 1660 event are indirectly compared by using empirical relationships between instrumental ground motion parameters and macroseismic intensities.

Ma after a rifting episode, which opened a narrow rift between the two plates (Choukroune 1992, and Olivet 1996, for reviews). The boundary between the two plates, the North Pyrenean fault, runs all along the range from west to east (Fig. 2). The present differential motion between the two plates is small, less than 1 mm yr^{-1} (Nocquet & Calais 2004). In agreement with this low deformation rate, the Pyrenean range is characterized by moderate seismicity. It is monitored by about 40 velocimeters and 30 accelerometers deployed on both the French and Spanish sides. About 600 to 800 events with $M_l > 1$ are located each year all along the range (Fig. 2). However, there are on average only one or two events with $M_l \geq 5$ every 10 yrs (Souriau & Pauchet 1998). Most of the focal depths are in the range of 4–12 km. The seismicity reveals a general E–W distribution, with complex fault systems (Gagnepain-Beyneix *et al.* 1982; Rigo *et al.* 1997, 2005; Ruiz *et al.* 2006).

Although the instrumental seismicity reveals only small to moderate earthquakes, the historical seismicity shows that the Pyrenees have been affected by strong earthquakes (Vogt 1979; Lambert & Levret-Albaret 1996). The period covered by the instrumental seismicity is short compared with the recurrence period of large earthquakes, which is of the order of centuries (Souriau & Pauchet 1998; Alasset & Meghraoui 2005). The instrumental seismicity thus gives an incomplete image of seismic hazard. For example, the strongest earthquake recorded in the eastern Pyrenees is a $M_l = 5.3$ event (St-Paul-de-Fenouillet in 1996, Rigo *et al.* 1997), with only minor damage, whereas the strongest reported historical event (north Catalonia in 1428) has an estimated magnitude of 6.4–6.5 (Lambert & Levret-Albaret 1996), and killed about 700 people. Historical seismicity is thus of major importance to bring further information for seismic hazard assessment.

Historical events are quantified with macroseismic intensities inferred from felt shaking and damage descriptions reported in historical documents. They allow us to derive maps of macroseismic intensities, isoseist contour lines and macroseismic epicentres.

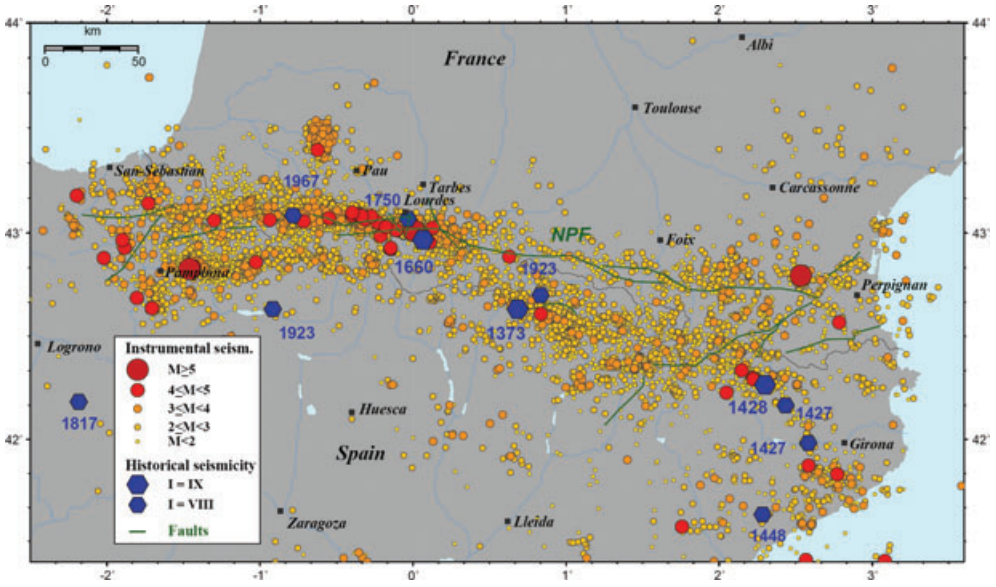

Figure 2. Instrumental seismicity for the period 1989–2009 (from Observatoire Midi-Pyrénées catalogues) and largest historical events with maximal MSK macroseismic intensity VIII and IX; NPF: North Pyrenean Fault.

Finally, by comparing the macroseismic maps of historical and instrumental events, it is possible to ascribe an equivalent magnitude to historical events (Levret *et al.* 1994). This magnitude may, however, be biased by numerous factors, such as the poor knowledge of the focal depth, the regional variations of attenuation, and different focal mechanisms.

French historical seismicity is well documented back to the 14th century, with about 25 events of maximum intensity greater than VII since the beginning of the 17th century (Lambert & Levret-Albaret 1996). Fig. 2 reports the main historical events in the Pyrenees, with their maximal intensity on the MSK scale (Medvedev *et al.* 1964). As with instrumental seismicity, historical events are distributed all along the range. The most important event on the French side occurred near Lourdes in 1660. We will now focus on this particular event.

2.2 The 1660 historical earthquake

On 1660 June 21, a major earthquake with a maximum MSK intensity of IX occurred in the central French Pyrenees. It is particularly well documented because there were populated areas in a wide area all around the epicentre. Moreover, it occurred just after the wedding of King Louis XIV in Saint-Jean-de-Luz in the western Pyrenees (Bernard *et al.* 1997). It is one of the most destructive Pyrenean earthquakes. As revealed by historical documents, it was felt in a large part of France, up to 500 km from the epicentre (Fig. 3). Part of the cities of Lourdes and Bagnères-de-Bigorre were destroyed, and about 30 deaths were reported. The suspected epicentral region is located about 17 km SE of Lourdes and 13 km SW of Bagnères-de-Bigorre (Figs 2 and 3). The macroseismic epicentre (42°58′N, 0°04′E) provided by the SisFrance catalogue (BRGM-IRSN-EDF *et al.* 2004) is given with an uncertainty of about 10 km. It is located inside an area of maximum intensity relatively well circumscribed by an isoseist (Fig. 3), and is thus rather reliable. The magnitude is estimated at $M_{\mathrm{l}} = 6.1 \pm 0.4$ (Levret *et al.* 1996) from empirical relationships established for French earthquakes (Levret *et al.* 1994). Cara *et al.* (2008) applied a differential macroseismic method based on the comparison between intensities of historical and recent instrumental earthquakes at large epicentral distances, to estimate the moment magnitude M_{w} of some historical earthquakes. For the 1660 event, they used the 2006 November earthquake as a reference and found a magnitude of $M_{\mathrm{w}} = 6.1 \pm 0.2$. This value ($M_{\mathrm{w}} = 6.1$) will be used for our simulations, we will discuss later the influence of this choice.

3 AN EMPIRICAL GREEN'S FUNCTION SIMULATION METHOD

To obtain realistic seismograms in a broad frequency range from our simulations we used an EGF approach (Hartzell 1978). A small, well-recorded event is chosen in the region of interest. Its recordings, called EGFs, are combined to produce realistic seismograms corresponding to a larger earthquake with the same focal mechanism. We assume that the recordings of the small event represent Green's functions at each point of the fault plane activated during the rupture of the large, simulated event. This approach takes directly into account both path and site effects at different stations, as they are included in the EGFs.

Among the possible EGF methods, we used a stochastic, two-step method proposed by Kohrs-Sansorny *et al.* (2005). The main advantage of this method is that it correctly provides the ω^{-2} model spectra (Aki 1967; Brune 1970) not only at low and high frequencies, but also in the transition region (between the corner frequencies of the small and large events). Moreover, it requires only a few input parameters, which is a great advantage for simulating an unknown event. This method has proved its efficiency for simulating the ground motions of moderate-size earthquakes, provided that a proper small event could be chosen as an EGF (Courboulex *et al.* 2010). It has also been recently used to simulate the effects of a rather large earthquake ($M_{\mathrm{w}} = 6.3$) in the southeast of France (Salichon *et al.* 2010).

This method is completely described in the paper of Kohrs-Sansorny *et al.* (2005). We give below an outline of the method, which is inspired by previous works of Joyner & Boore (1986), Wennerberg (1990) and Ordaz *et al.* (1995). The overall principle is simple: a large number of time histories called 'Equivalent Source

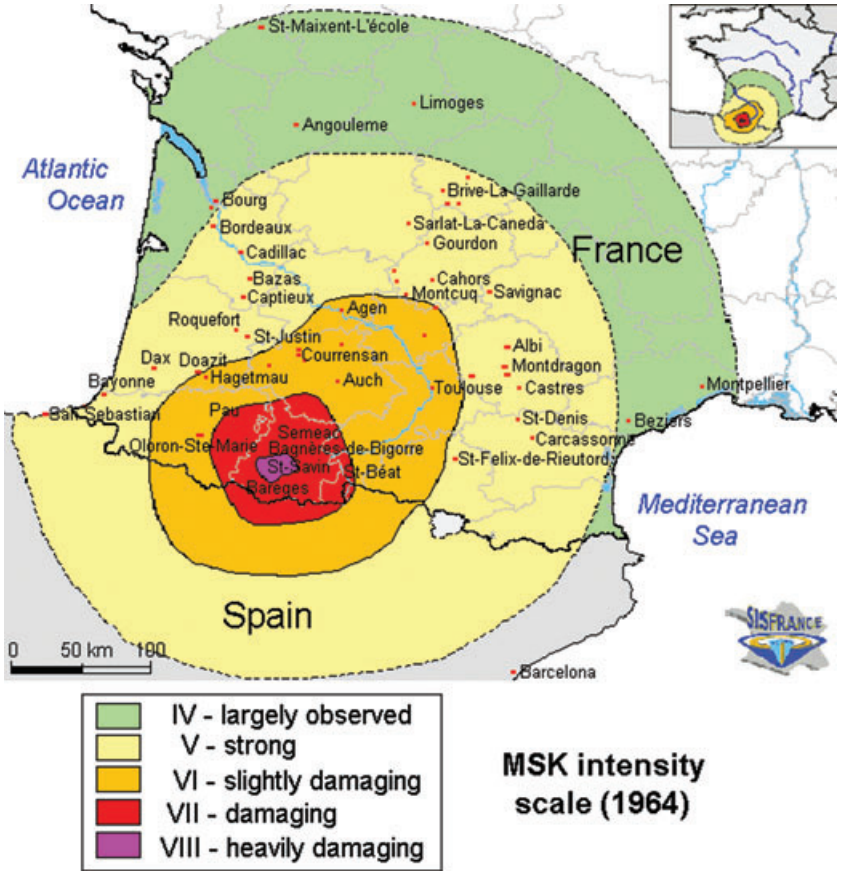

Figure 3. Isoseists contour lines and intensity domains (on MSK scale, 1964) for the 1660 historical earthquake (SisFrance catalogue, BRGM *et al.* 2004).

Time Functions' (ESTFs) are generated. Each ESTF, representative of a given rupture process, is convolved with the small-event records to provide the synthetic signals. The ESTFs are built using a random process based on probability densities as proposed by Ordaz *et al.* (1995), which ensures the generation of the ω^{-2} model spectra at all frequencies. The source frequency content must, on average, explain the theoretical ratio $R(f)$ between the spectra of the large and small events

$$R(f) = \frac{M_0}{m_0} \cdot \frac{\left(1 + \left(\frac{f}{f_c}\right)^2\right)}{\left(1 + \left(\frac{f}{F_c}\right)^2\right)}. \quad (1)$$

A particularity of the method developed by Kohrs-Sansorny *et al.* (2005) is the generation of the ESTFs in two stages: in the first stage, a number η_c of delays t_c are randomly generated with a probability density $\rho_c(t)$ over the whole source duration T_c. T_c is deduced from the corner frequency F_c of the main event: $T_c = 1/F_c$. In the second stage, a number η_d of delays t_d are again generated with a second probability density $\rho_d(t)$ over a window duration $T_d \leq T_c$ centred on each delay generated in the first stage. Finally, $\eta = \eta_c \cdot \eta_d$ small events are summed together and scaled by a factor κ (eq. 2a).

$$\mathrm{ESTF}_k(t) = \kappa \sum_{d=0}^{\eta_d - 1} \left[\sum_{c=0}^{\eta_c - 1} \delta(t - t_c - t_d) \right] \quad (2a)$$

By an appropriate choice of the parameters η and κ (eq. 2b), the method produces time histories that statistically explain eq. (1), and respect a non-constant stress drop condition (Beeler *et al.* 2003; Kanamori & Rivera 2004).

$$\eta = \eta_c \cdot \eta_d = N^4 \text{ and } \kappa = \frac{C}{N}, \quad (2b)$$

where:

$$N = \frac{f_c}{F_c},\ C = \frac{\Delta\Sigma}{\Delta\sigma} \text{ and } T_c = \frac{1}{F_c}$$

The parameter C represents the stress drop ratio between the large and the small earthquake. $C = 1$ implies that the target event and the small event have the same stress drop. Many studies have shown that the stress drop may vary from one event to another, and that it has a large influence on the generation of strong motions. It is then important to allow some variability for this parameter. N is equal to the ratio between the corner frequency of the small event f_c and that of the large event F_c. In practice N will be set as an integer, which implies that only discrete values of F_c, thus discrete values of C, will be possible.

Compared with the single-stage summation proposed by Ordaz *et al.* (1995), the time histories produced using the two-step method have larger variability (Kohrs-Sansorny *et al.* 2005). This is particularly important when N is high, that is, when the magnitude of the target event is large compared to the magnitude of the small event taken as an EGF, as is the case in our study. In this paper, we chose $\eta_c = \eta_d = N^2$, that is, an equal distribution of the two steps in the summation process.

One important feature of this method is that the number of input parameters is small. Indeed, the only parameters that need to be specified are: (1) the seismic moment (m_0) and the corner frequency

(f_c) of the small event taken as an EGF, which are directly determined from the data; (2) the seismic moment (M_0) of the target event; (3) the ratio C between the static stress drop of the target event ($\Delta\Sigma$) and that of the small event ($\Delta\sigma$). These parameters are linked by the relationship

$$CN^3 = \frac{M_0}{m_0}. \quad (3)$$

The main difficulty is to define the range of possible values of C that need to be investigated. We will discuss this point further in this paper.

4 DATA

4.1 Data selection and network

Instrumental data of two recent Pyrenean earthquakes are used: the 2006 November 17, earthquake ($M_l = 5.0$) (Sylvander *et al.* 2008) and the 2007 November 15, earthquake ($M_l = 4.1$). They occurred almost at the same location, and have very similar characteristics (Table 1). The distance between the two epicentres is less than 1 km and the difference in depths is about 2 km. They have similar normal fault mechanisms. They occurred a few kilometres south of the North Pyrenean Fault on an east–west oriented fault. This tectonic structure, previously identified by Rigo *et al.* (2005), is suspected to be responsible for the 1660 historical earthquake. These two earthquakes thus satisfy all the requirements to be used as EGFs in our simulation of the 1660 event. Moreover, these earthquakes were recorded with a good signal-to-noise ratio by a large number of accelerometric stations of the French Permanent Accelerometric Network (Pequegnat *et al*. 2008). For this study we selected 11 accelerometric stations at epicentral distances lower than 100 km. Their local site geology is based on superficial geological considerations, with a simplified soil classification into two categories: rock sites and sedimentary sites (see: http://www-rap.obs.ujf-grenoble.fr) (Table 2; Fig. 4).

4.2 Data analysis for determination of the input parameters

The simulation method requires the knowledge of a few input parameters, which can be determined from an analysis of the data of the two selected earthquakes. The parameters we need are the seismic moment, the corner frequency and the static stress drop ratio.

4.2.1 Seismic moment

For the 2006 earthquake, we took the seismic moment determined by Sylvander *et al.* (2008): $M_0 = 5.32 \times 10^{15}$ (N m), corresponding to a moment magnitude $M_w = 4.48$. To determine the seismic moment of the 2007 earthquake, we used the spectral ratio between the recordings of the 2006 and the 2007 earthquakes. We obtained a moment of $m_0 = 2.38 \times 10^{14}$ (N m) for the 2007 earthquake, which corresponds to a moment magnitude $m_w = 3.58$. As previously observed by Drouet *et al.* (2005) for moderate Pyrenean earthquakes, moment magnitudes M_w are about 0.5 units smaller than local magnitudes M_l. Such differences are often observed and may have various origins, in particular the way M_l is measured, and the way attenuation along the path is corrected (Deichmann 2006).

4.2.2 Corner frequency

The corner frequencies of the 2006 and 2007 earthquakes are determined from displacement spectra assuming an ω^{-2} source model (Brune 1970). The low- and high-frequency sides of the Fourier amplitude spectra are fitted with the ω^0 and ω^{-2} asymptotes respectively, and the corner frequency is given by their intersection. For the 2007 earthquake ($M_w = 3.6$), the value of the corner frequency is almost the same at all stations, with an average value $f_c = 3.3 \pm 0.3$ Hz. The situation is quite different for the 2006 earthquake ($M_w = 4.5$): the corner frequency appears clearly dependent on the backazimuth of the station (Fig. 5). The robustness of this observation is confirmed from the analysis of the spectral ratios of the

Table 1. Hypocentral locations and focal mechanism parameters (from Sylvander *et al.* 2008) of the two instrumental earthquakes used in this study.

			Hypocentral location			Focal mechanism		
			Lat. (°)	Long. (°)	Depth (km)	Plane 1		
Date	Time (UTM)	M_l				Strike (°)	Dip (°)	Rake (°)
2006 November 17	18 h19 m 51 s	5.0	43.0282	0.0032	9.7	284	56	–84
2007 November 15	13 h 47 m 35 s	4.1	43.0207	0.0022	7.8	296	30	–50

Table 2. Location and local site geology of the Pyrenean accelerometric stations used in this study. All of them belong to the French Permanent Accelerometric Network (see: http://www-rap.obs.ujf-grenoble.fr).

Station name	Locality	Latitude (°)	Longitude (°)	Elevation (m)	Local site geology
PYAD	Arudy	43.098	–0.426	450	Rock
PYAS	Aspet	43.012	0.797	430	Sediment
PYAT	Arette	43.095	–0.711	340	Rock
PYBB	Bagnères-de-Bigorre	43.059	0.149	560	Rock
PYLI	St Lizier	43.002	1.136	424	Rock
PYLO	Lourdes	43.098	–0.048	410	Rock
PYLS	Luz-St-Sauveur	42.860	–0.009	770	Rock
PYLU	Luchon	42.791	0.601	630	Sediment
PYPC	Pau (castle)	43.296	–0.374	200	Rock
PYPU	Pau (university)	43.315	–0.366	208	Sediment
PYTB	Tarbes	43.226	0.049	305	Sediment

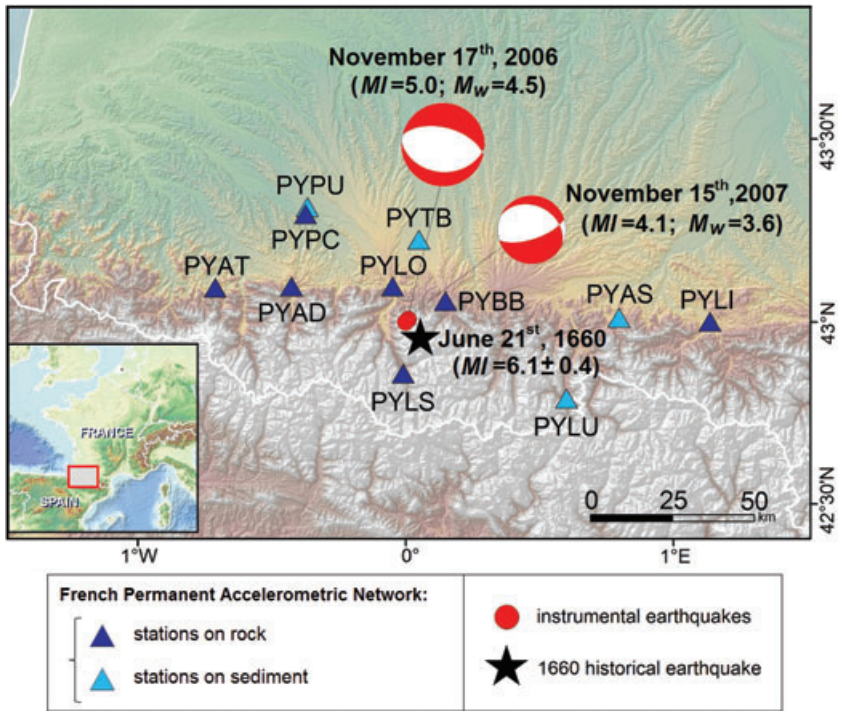

Figure 4. Epicentres (red dots) and focal mechanisms of the two selected instrumental earthquakes (Sylvander *et al.* 2008) and location of the 11 Pyrenean accelerometric stations used in this study. Stations on rock and sediment are indicated with different colours. Black star: macroseismic epicentre of the 1660 historical earthquake, given with a location uncertainty of about 10 km (SisFrance catalogue, BRGM *et al.* 2004).

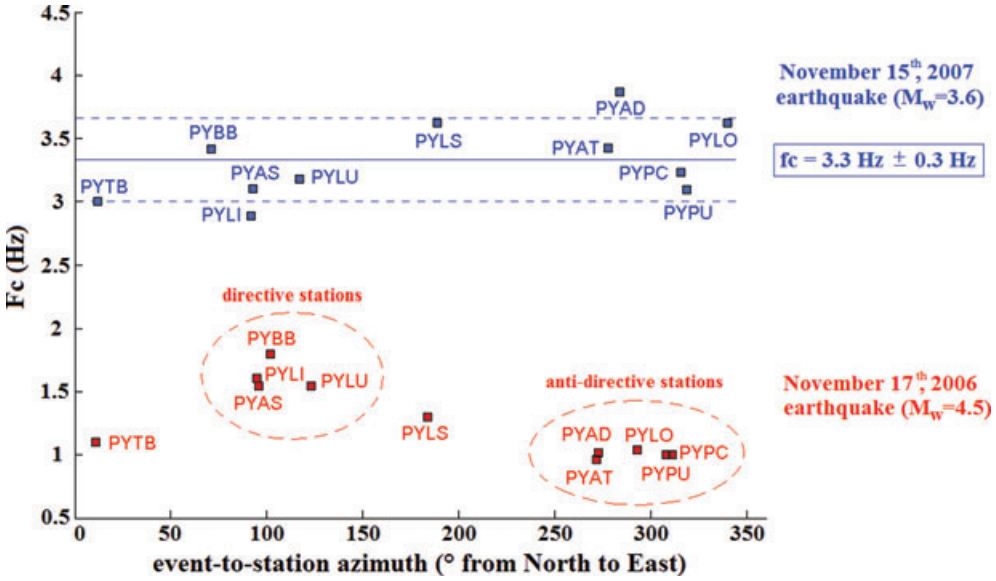

Figure 5. Corner frequencies obtained at each station from displacement spectra analysis as a function of station backazimuth for the 2007 November earthquake ($M_w = 3.6$) and the 2006 November earthquake ($M_w = 4.5$). For the first earthquake the values obtained are rather stable with azimuth, with an average value (blue line) of 3.3 Hz and a standard deviation (dotted blue lines) of 0.3 Hz. For the second earthquake a clear dependency of the corner frequency with azimuth is observed. It can be explained by the directivity of the rupture.

two events, an approach that theoretically eliminates path and site effects that could affect source parameter determination.

4.3 Directivity effect of the $M_w = 4.5$ earthquake

The apparent dependence of the corner frequency on backazimuth suggests a directivity in the rupture of the $M_w = 4.5$ event. We distinguish the true and apparent rupture durations, $T_c = 1/F_c$ and $T_a = 1/F_a$, where F_c and F_a are the true and apparent corner frequencies. We assume a simple line source model with unilateral rupture propagation at a constant velocity V_r. It is related through the following expression

$$T_a = T_c - T_c V_R \frac{\cos(\theta - \theta_0)}{c}, \quad (4)$$

where θ and θ_0 are the azimuths of the station and the rupture propagation respectively, V_r is the rupture velocity, c is the wave

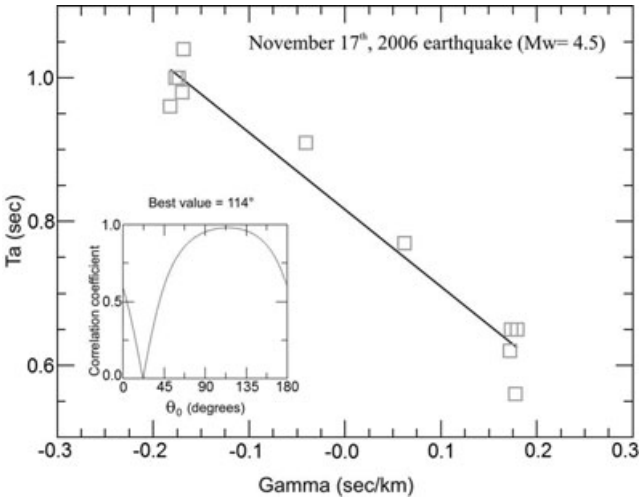

Figure 6. Directivity analysis of the 2006 November earthquake (M_w = 4.5). The inset shows the variation of the linear correlation coefficient between observed and computed corner frequencies as a function of azimuth of rupture propagation (angle θ_0). The largest correlation value is found for directivity N114E°. For this selected value of the source azimuth, the figure shows a plot of apparent source time function duration (T_a) as a function of the directivity factor Gamma (Γ).

velocity near the source and T_c is the actual source duration. For a directive station ($\theta - \theta_0 = 0°$), the apparent rupture duration is shorter than for an antidirective station ($\theta - \theta_0 = 180°$), which results in larger ground motion amplitudes for a directive station than for an antidirective station.

Eq. (4) can be rewritten as

$$T_a = T_c - \Gamma L, \tag{5}$$

where $L = T_c\, V_r$ represents the horizontal length of the rupture and $\Gamma = \cos(\theta - \theta_0)/c$ the directivity factor.

We systematically varied the values of θ_0 to obtain the best linear correlation characterizing the dependence of T_a on θ_0. A very good correlation coefficient of 0.97 is obtained for $\theta_0 = 114°$ (Fig. 6). This result is in good agreement with the focal mechanism and the azimuth of the main faults in the region. Fig. 6 gives a plot of T_a as a function of Γ for this θ_0 value. From this figure we obtained the duration of the rupture process $T_c = 0.81$ s (for $\Gamma = 0$), and the length of the fault, $L = 1$ km, from the slope. These values are realistic for such an earthquake, but they imply a slow rupture propagation, $V_r \sim 1.25$ km s^{-1}.

Finally, the stations can be classified into two main groups: directive stations in the rupture direction to the east (PYAS, PYBB, PYLI, PYLU) and antidirective stations to the west (PYAD, PYAT, PYLO, PYPC, PYPU, PYTB). PYLS can be considered as a non-directive station.

5 GROUND MOTION SIMULATIONS OF THE M_w = 4.5 EVENT FROM THE M_w = 3.6 EVENT: A VALIDATION TEST

5.1 How to take into account the directivity effect?

We first aimed to reproduce the ground motions generated by the 2006 earthquake (M_w = 4.5) by using the 2007 earthquake (M_w = 3.6) as an EGF. This led us to investigate how the directivity effect of a target event could be taken into account in our simulation method. Note that we focus here on this particular 2006 event, but we do not aim to simulate the whole variability of the ground motions for any M_w = 4.5 earthquake (as this will be the case in Section 6 for the blind simulation of an M_w = 6.1 event).

Table 3. Fixed input parameters for the simulation of the 2006 earthquake (M_w = 4.5) by using the 2007 earthquake (M_w = 3.6) as an empirical Green's function. F_c is the corner frequency and C the static stress drop ratio.

Date	M_w	F_c (Hz)	C
2006 November 17	4.5	1.2	1.07
2007 November 15	3.6	3.3	

Table 4. Apparent corner frequency F_a obtained at each station from data analysis of the 2006 earthquake (see Fig. 5) and input parameters used to include the directivity effect of the target event. C_a parameter is consistent with an N integer condition.

Station	Az (°)	F_a (Hz)	N	C_a
PYLI	95	1.60	2	2.79
PYAS	96	1.54	2	2.79
PYBB	102	1.80	2	2.79
PYLU	123	1.54	2	2.79
PYLS	184	1.30	2	2.79
PYAT	272	0.96	3	0.83
PYAD	273	1.02	3	0.83
PYLO	293	1.04	3	0.83
PYPC	308	1.00	3	0.83
PYPU	311	1.00	3	0.83
PYTB	11	1.10	3	0.83

Among the four necessary input parameters, we considered as fixed parameters the moment magnitude of the target earthquake M_w, the moment magnitude m_w and the corner frequency f_c of the small earthquake taken as an EGF (Table 3). Their values were determined in Section 4.2. The last input parameter needed is the ratio C between the static stress drops of the two events. According eq. (3), the stress drop ratio parameter C can also be expressed as a function of corner frequency F_c of the target earthquake

$$C = \left(\frac{M_0}{m_0}\right)\left(\frac{F_c}{f_c}\right)^3. \tag{6}$$

Using the rupture duration of the 2006 earthquake as determined in Section 4.3, which corresponds to a corner frequency F_c = 1.2 Hz, we obtained a stress drop ratio C = 1.07. However, if we set this value as an input parameter for all the stations, we are not able to reproduce the directivity of the target event. We thus introduced a new input parameter C_a, which is a function of T_a, the apparent rupture duration at a given station

$$C_a = \left(\frac{T_r}{T_a}\right)^3 \cdot C \tag{7}$$

For each station, the input parameter C_a was adjusted depending on the location of the station with respect to the directivity of the rupture. As the corner frequency ratio N is set as an integer, only discrete values of C_a could be used. Therefore, we ran simulations for which C_a took two different values: C_a = 2.79 (N = 2) for directive stations and C_a = 0.83 (N = 3) for antidirective stations (Table 4). This implies that we simulated an earthquake with apparent rupture durations of T_a = 0.61 s for directive stations and T_a = 0.91 s for antidirective stations.

This approach enabled us to simulate a simple directivity effect for a given station with only a variation of the duration of the apparent source time function. For a point source approximation this is equivalent to varying the static stress drop on the fault.

5.2 Simulation results and comparison with the data

Using the parameters given in Tables 3 and 4, we simulated the three-component accelerograms for 500 different earthquakes of magnitude $M_w = 4.5$ at the 11 stations, by using the 2007 earthquake ($M_w = 3.6$) as an EGF. Examples of synthetic accelerograms for the E–W component are shown at four stations in Fig. 7, together with the EGF and the observed records. The corresponding amplitudes of the Fourier displacement spectra are shown in Fig. 8. The fit between synthetic and observed records is good in a broad frequency range. Note that at frequencies lower than 0.1 Hz, the signal of the small event is dominated by noise and cannot be taken into account for the simulations.

Simulation results are also analysed in terms of elastic acceleration response spectra. They describe the maximum response of a Single Degree of Freedom system to a particular input motion, as a function of the natural period and damping ratio of the system. From the synthetic accelerograms, we computed the response spectra with 5 per cent damping for each component at each station. Median spectral accelerations and 16th and 84th percentiles (which correspond to $\pm\sigma$, one standard deviation for a logarithmic representation), are computed to characterize ground motion variability in our simulations. The comparison between observed and simulated acceleration response spectra (Fig. 9) shows that the 2006 earthquake ground motions are well reproduced by our simulations. Note that the adjustment of a different input parameter C_a for directive and antidirective stations was necessary to provide ground motion amplitudes consistent with the rupture directivity. Ignoring the directivity would have led to a clear underestimation of ground motions for the eastern stations, or to an overestimation for the western stations (Fig. 10).

Fig. 11 compares the peak ground accelerations (PGA) recorded during the 2006 earthquake and those obtained from simulations. The agreement is generally very good. It is clear that the directivity effect has a strong influence on the PGA values, as mentioned by other authors for small earthquakes (Boatwright 2007). In our example, the influence of directivity is as important as that of site effects on the PGA. The combined effects of directivity and site conditions can be observed at PYAT and PYLU stations which are located at the same epicentral distance. PYAT is located on rock and is antidirective whereas PYLU is on sediment and is directive. Its PGA value is five times larger than at PYAT. Our simulations generally reproduce these effects quite well, even though the directivity is only approximately taken into account, due to the discrete values imposed on the directivity factor C_a. By contrast, the site effect is exactly modelled because it is contained in the small earthquake used as an EGF.

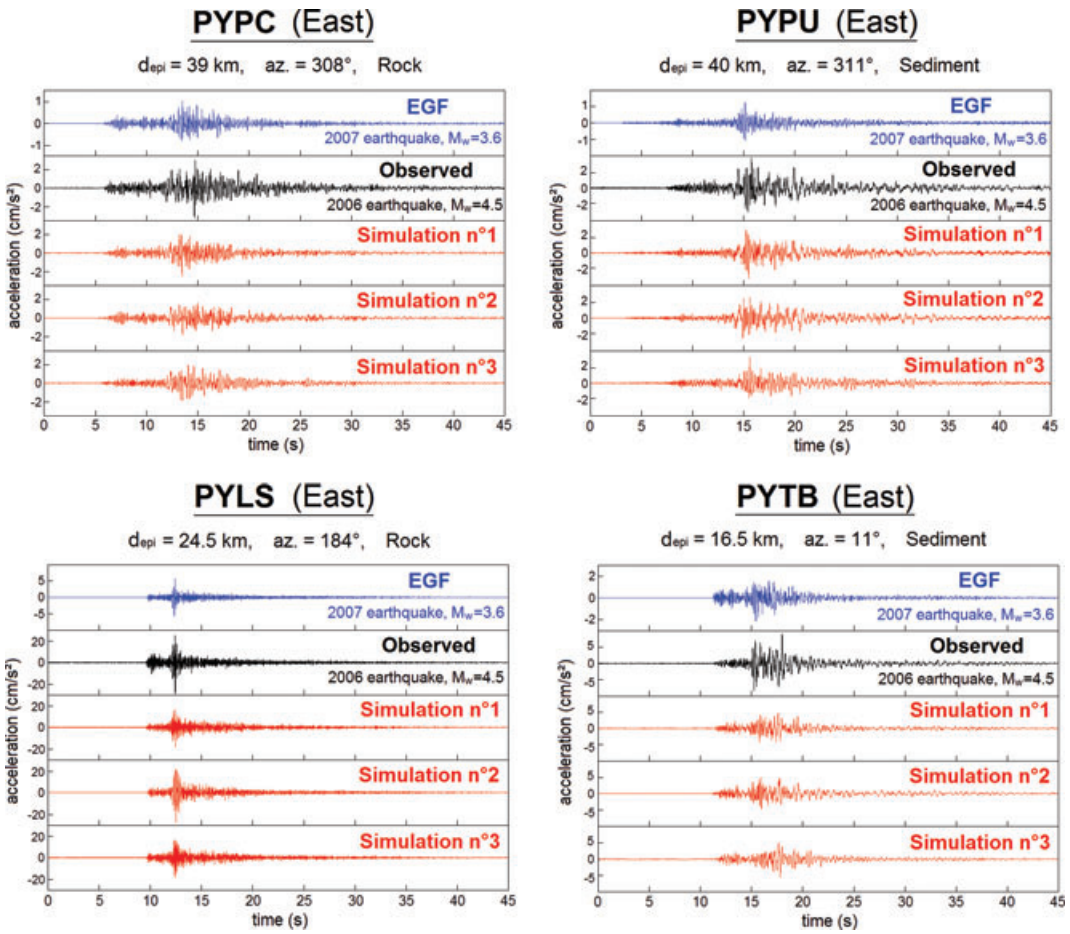

Figure 7. Accelerograms of the observed 2006 earthquake (in black) compared with a sample of three simulations (in red) out of the 500 generated at four stations (PYPC, PYPU, PYLS and PYTB) and accelerograms of the 2007 earthquake used as an EGF (in blue).

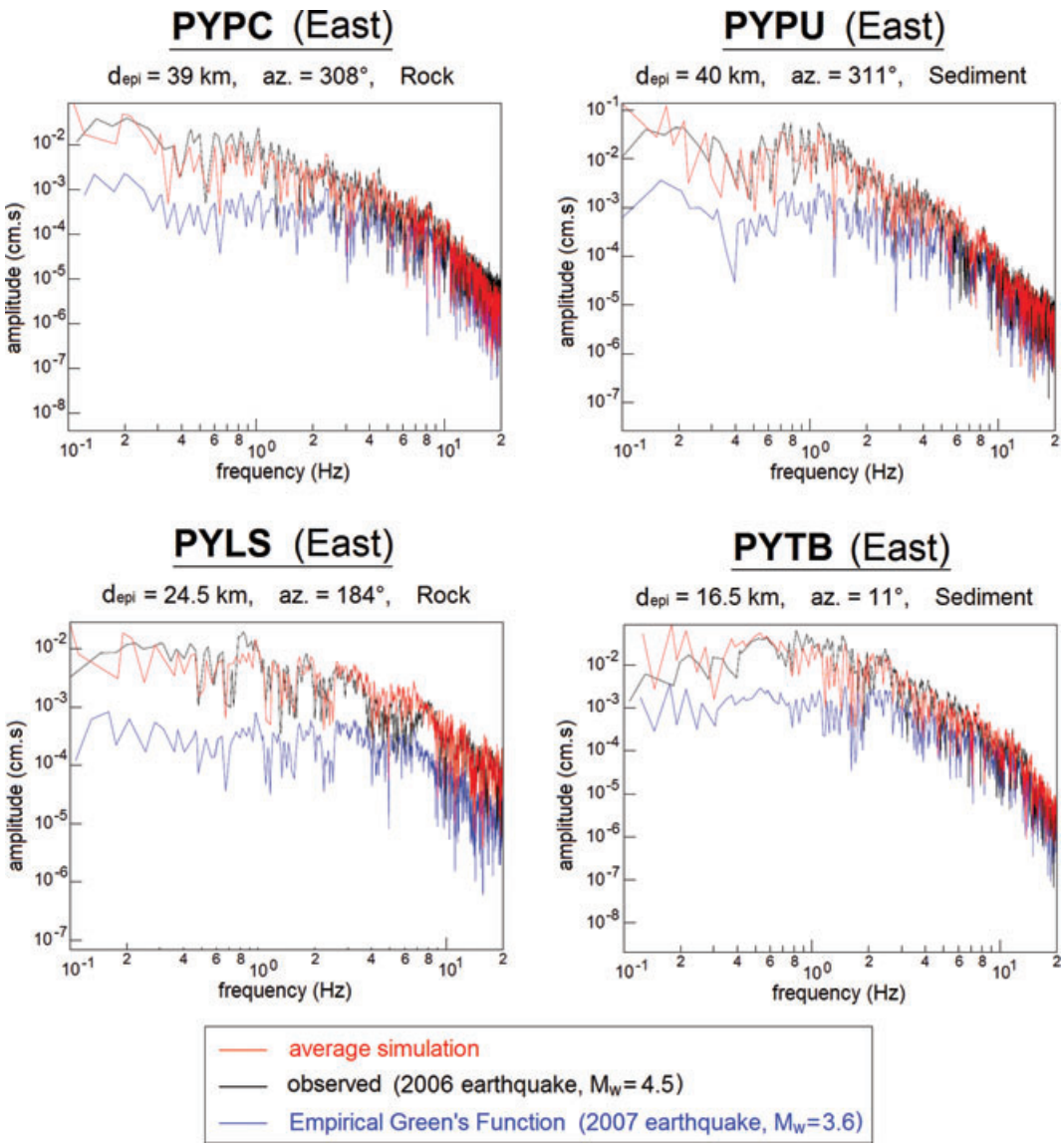

Figure 8. Fourier displacement spectra of the observed 2006 earthquake (in black) at four stations (PYPC, PYPU, PYLS and PYTB) compared with an average simulation (in red) and displacement spectra of the 2007 earthquake used as an EGF (in blue).

This simulation of the 2006 event with a 'station-dependent' stress drop ratio was possible because the directivity of the 2006 event was clearly identified. The simulation of the 1660 event (Section 6), for which the directivity is unknown, will require a blind approach: the directivity will be indirectly modelled by repeating calculations with different stress drop ratios (the same at all stations) that aim to account, in a statistical sense, for the source variability of an $M_w = 6.1$ earthquake.

6 GROUND MOTION SIMULATIONS OF AN $M_w = 6.1$ EARTHQUAKE FROM THE $M_w = 3.6$ EVENT

6.1 A case of blind simulation

We aimed to simulate the ground motion that could result from a magnitude $M_w = 6.1$ earthquake, equivalent to the 1660 Pyrenean historical event. We decided to use only the 2007 earthquake ($M_w = 3.6$) as an EGF, because it is not affected by the directivity effect. If the 2006 event ($M_w = 4.5$) was chosen as an EGF, it would first be necessary to compensate for the directivity effect; otherwise the target event would reproduce this effect. We will discuss later how to indirectly account for the possible source variability of the target event.

The moment magnitude M_w of the target event, the moment magnitude m_w and the corner frequency f_c of the small earthquake used as an EGF are fixed input parameters. The other input parameter, the static stress drop ratio C, is difficult to define, as we have no *a priori* constraint on the static stress drop of the $M_w = 6.1$ target event. We thus ran different simulations for which the stress drop ratio parameter C is set at different values between 0.38 and 3.43 (consistent with an N integer condition). We selected values that enable us to reproduce a lognormal distribution of PGA. This range of C values corresponds to rupture durations between 3.6 and 7.6 s for the target event, which are reasonable values for such an earthquake (Houston 2001; Table 5). Note that we included stress drop ratios both lower and higher than 1.0, assuming no particular dependence of stress drop on seismic moment, as the stress drop scaling with

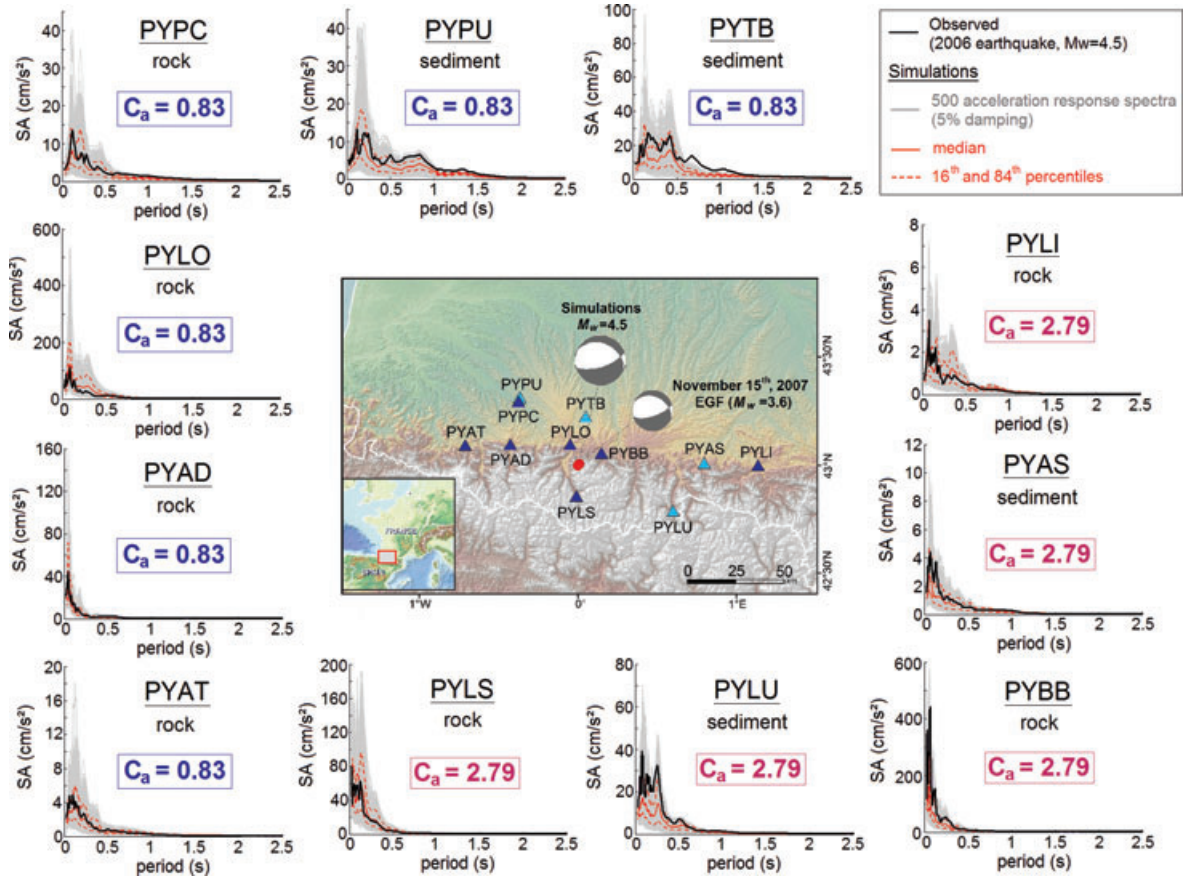

Figure 9. Elastic response spectra in acceleration of the observed 2006 earthquake (in black) at each station, for the eastern component. Superimposed are the median and 84th–16th percentiles (in red) computed from 500 acceleration response spectra (in grey). The parameter C_a is adjusted depending on the location of the station with respect to the directivity of the rupture: $C_a = 2.79$ for directive stations and $C_a = 0.83$ for antidirective stations.

magnitude remains debated (e.g. Ide & Beroza 2001; Allmann & Shearer 2009).

For each value of C, we produced for each station a set of 500 different synthetic accelerograms that could be generated by an $M_w = 6.1$ earthquake. As seven different values of C are tested, we obtained a total of 3500 simulations for each station and each component. Fig. 12(a) shows the influence of the stress drop ratio parameter C on ground motion amplitudes: spectral acceleration levels increase with increasing C values. To characterize the ground motion variability resulting from the unknown stress drop, we computed for each period a median value of the spectral accelerations and the 84th–16th percentiles, which correspond to one standard deviation (Fig. 12b).

6.2 Simulation results

Fig. 13 shows the ground motion levels, in terms of spectral accelerations and PGA, obtained from our simulations. The highest spectral accelerations and PGA values are obtained at station PYLO (on rock) located in the city of Lourdes. The median PGA value is equal to 172 cm s^{-2}, and the 84th percentile leads to a value of 347 cm s^{-2} for PGA at this station. Note that this station has an epicentral distance of only 9 km, which is theoretically at the limit of application of EGF simulation methods (Irikura & Kamae 1994). We also estimated ground motions at stations located in the largest cities of the region. For station PYTB (on sediment) located in the city of Tarbes at an epicentral distance of 23 km, a median PGA value of 54 cm s^{-2} is obtained. A local site effect is observed, with in particular a peak in acceleration at period $T \sim 0.4$ s. In the city of Pau, at an epicentral distance of about 43 km, we obtained respectively for the stations PYPC (on rock) and PYPU (on sediment) median PGA values of 20 cm s^{-2} and 24 cm s^{-2}. They are almost the same at both stations in spite of different soil conditions, but the shapes of response spectra are different, with an amplification at period $T \sim 0.8$ s at PYPU. The comparison of the spectra at the two stations, PYAT (on rock) and PYLU (on sediment), located at the same epicentral distance, reveals spectral accelerations and PGA values twice as large at PYLU as at PYAT. We also note that station PYAD exhibits unexpected high spectral accelerations and PGA values, for an epicentral distance of 35 km. This station, located on rock at the top of a crest, is subject to a topographic site effect, which amplifies the high frequencies (Drouet *et al.* 2007).

In recent seismic hazard assessment studies, the acceleration levels expected for this region of the Pyrenees differ significantly from one study to another. Dubos *et al*. (2004) extrapolated PGA values obtained at PYLO for different magnitudes after attenuation correction. They estimated a maximum horizontal PGA of 100 ± 20 cm s^{-2} at Lourdes (on rock) for a magnitude 6 earthquake occurring 10 km from the city. Marin *et al.* (2004) performed a probabilistic seismic hazard assessment for the French home territory, they obtained a maximum horizontal PGA around 67 cm s^{-2} for a 475-yr return period (which corresponds to a 10 per cent probability of over-passing this acceleration in 50 yr). In a probabilistic seismic hazard assessment for the Pyrenean region using both French and

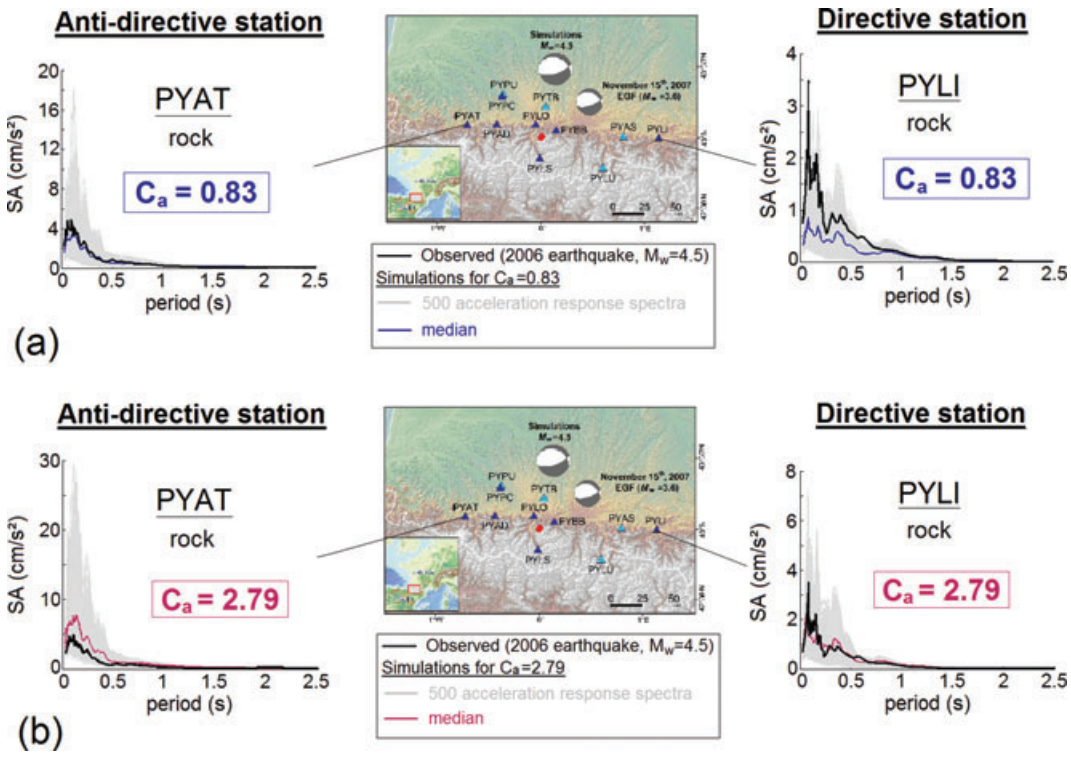

Figure 10. Examples of simulation results for PYAT and PYLI stations (eastern component) when the C_a parameter is not adjusted to account for the directivity of the rupture. (a) When C_a is set to 0.83, we obtain an underestimation of the observed ground motions (in black) for the directive station PYLI; (b) When C_a is set to 2.79, we obtain an overestimation of observed ground motions (in black) for the antidirective station PYAT.

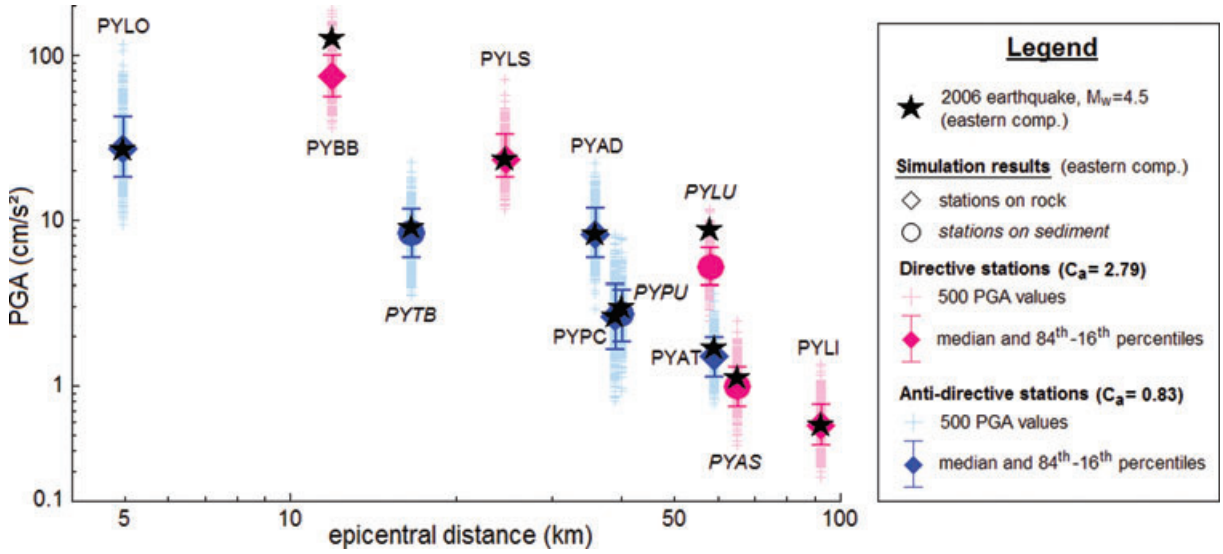

Figure 11. PGA values observed for the 2006 earthquake (black stars) as a function of epicentral distance, compared with the median PGA values and 16th–84th percentiles computed from 500 simulations at each station (eastern component). Note the influence of the directivity, which induces higher PGAs for the directive stations (in red) than for the antidirective ones (in blue).

Spanish data, Secanell *et al.* (2008) come to higher values, with a median PGA up to 150–200 cm s^{-2} for a 475-yr return period. Our acceleration results for the simulation of the $M_w = 6.1$ event are thus globally in fair agreement with previous published results.

6.3 Comparison with Ground Motion Prediction Equations (GMPEs)

A validation of our simulation may be made by comparing our results with different empirical GMPEs. As the low seismic activity in France does not allow to derive a specific GMPE, we used GMPEs obtained for other regions in the world. Over the years, a large number of GMPEs have been proposed (Douglas 2003) and one of the difficulties is to select a GMPE that could be appropriate for the Pyrenees. In the study of Drouet *et al.* (2007), eight published GMPEs adapted to shallow crustal events were tested for their applicability to Pyrenean earthquakes, by using the method of Scherbaum *et al.* (2004). Among the studied empirical models, they found that the GMPE developed by Lussou *et al.* (2001)

Table 5. Input parameters for the simulation of the $M_w = 6.1$ earthquake by using the 2007 earthquake ($M_w = 3.6$) as an EGF. The moment magnitude M_w of the target event, the moment magnitude m_w and the corner frequency f_c of the EGF are fixed input parameters. The static stress drop ratio C is a variable input parameter taking seven different values in the range [0.38 3.43]. T_r is the corresponding rupture duration value.

Fixed input parameters		
M_w	m_w	f_c (Hz)
6.1	3.6	3.3
Variable input parameter		
C	T_r (s)	
0.38	7.57	
0.43	7.27	
0.74	6.06	
1.02	5.45	
1.45	4.85	
2.16	4.24	
3.43	3.64	

from Japanese K-net data is the best-ranked GMPE (quality class B) for Pyrenean earthquakes, whereas the other ones over-predict the observed ground accelerations. The GMPEs of Berge-Thierry *et al.* (2003) and Ambraseys *et al.* (1996), which are usually used in seismic hazard studies in France, are respectively ranked as 'acceptable' (class C) and 'unacceptable' (class D). However, as noted by the authors, the GMPEs were evaluated by applying the method to low-magnitude earthquakes ($M_w \leq 4.0$).

We finally decided to compare our simulation results with the GMPEs of Lussou *et al.* (2001), Berge-Thierry *et al.* (2003) and Ambraseys *et al.* (2005) (Table 6). The latter are developed for estimation of PGA and pseudospectral accelerations (with 5 per cent damping). All these GMPEs include soil class as an explanatory variable, with a site classification based on the shear velocity average over the uppermost 30 m (V_{S30}). Ambraseys *et al.* (2005) also incorporate style-of-faulting as an explanatory variable. Each GMPE uses different magnitude and distance definitions, thus modifications must be considered to account for these disparities. The GMPE of Ambraseys *et al.* (2005) directly uses moment magnitude M_w, whereas the GMPEs of Lussou *et al.* (2001) and Berge-Thierry *et al.* (2003), respectively use Japanese Meterological Agency magnitude M_J and surface-wave magnitude M_S. However, for a value of moment magnitude M_w of about 6.0, it is found that M_J, M_S and M_w are close to each other (Heaton *et al.* 1986). For source-to-site distance definition, Ambraseys *et al.* (2005) use the Joyner & Boore (1981) distance to the surface projection of the fault. In our study, the fault dimension of the target earthquake is unknown, so we use epicentral distances instead.

Fig. 14 shows the comparison between the PGA values obtained from our simulations and those predicted by the selected GMPEs for an $M_w = 6.1$ earthquake. For each station, median and 84th–16th percentile PGA values are compared with the PGA levels predicted by the GMPEs, as a function of source-to-site distance. For Lussou *et al.* (2001) and Berge-Thierry *et al.* (2003) GPMEs, both the north–south and the east–west components are shown. For Ambraseys *et al.* (2005), only the largest PGA-value from the two horizontal components is given. The empirical equations used are those corresponding to rock site condition, whereas for simulation results both stations on rock and sediment are represented.

Globally, our simulation results are in good agreement with the three GMPEs up to a distance of 60 km. This successful result is an important validation of our simulations. A very good agreement is obtained with the equation of Ambraseys *et al.* (2005), whereas our results are slightly above the GMPE of Lussou *et al.*, and slightly below that of Berge-Thierry *et al*. (2003). Moreover, the PGA standard deviations obtained for the simulations and those predicted by the GMPEs are similar. This indicates that varying the C parameter in our simulations successfully reproduces (in a statistical sense) the variability of stress drop and directivity of the real earthquakes of similar magnitudes ($M_w \sim 6.1$). These results are thus quite encouraging. Note that a detailed study of the standard deviations obtained from simulations can be found in Beauval *et al.* (2009) using that same method but another database.

For distances greater than 60 km, all GMPEs supply PGA values higher than those obtained from simulations. As our simulations are based on recordings of a small magnitude event ($M_w = 3.6$), the latter observation can be explained by a decay rate of ground motion peak value with distance dependent on the magnitude. Indeed, PGAs from small events attenuate faster with distance than those generated from large events (e.g. Ambraseys *et al.* 2005; Bragato & Slejko 2005; Cotton *et al.* 2008).

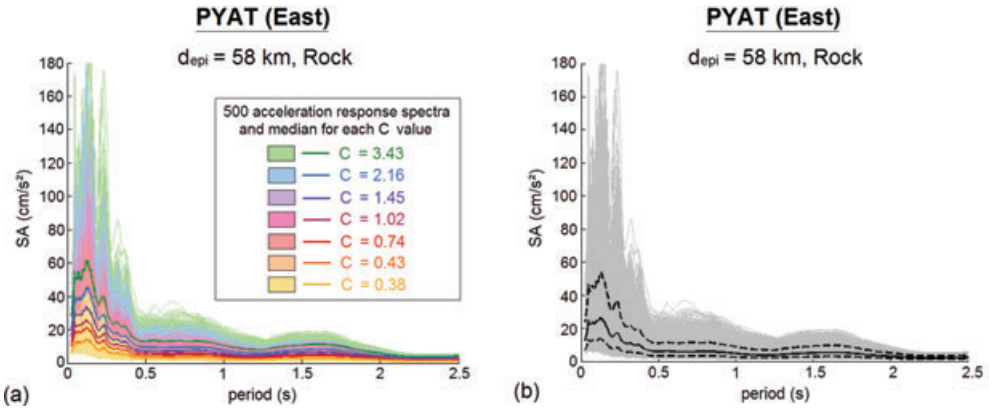

Figure 12. (a) Seven sets of 500 acceleration response spectra (5 per cent damping) obtained for each stress drop ratio parameter C, tested for the simulation of a $M_w = 6.1$ earthquake at station PYAT (eastern component). Median spectral accelerations computed for each C value are superimposed; (b) Overall spectral acceleration distribution including an uncertainty on the stress drop ratio parameter C (in grey) and median with 84th–16th percentiles (in black).

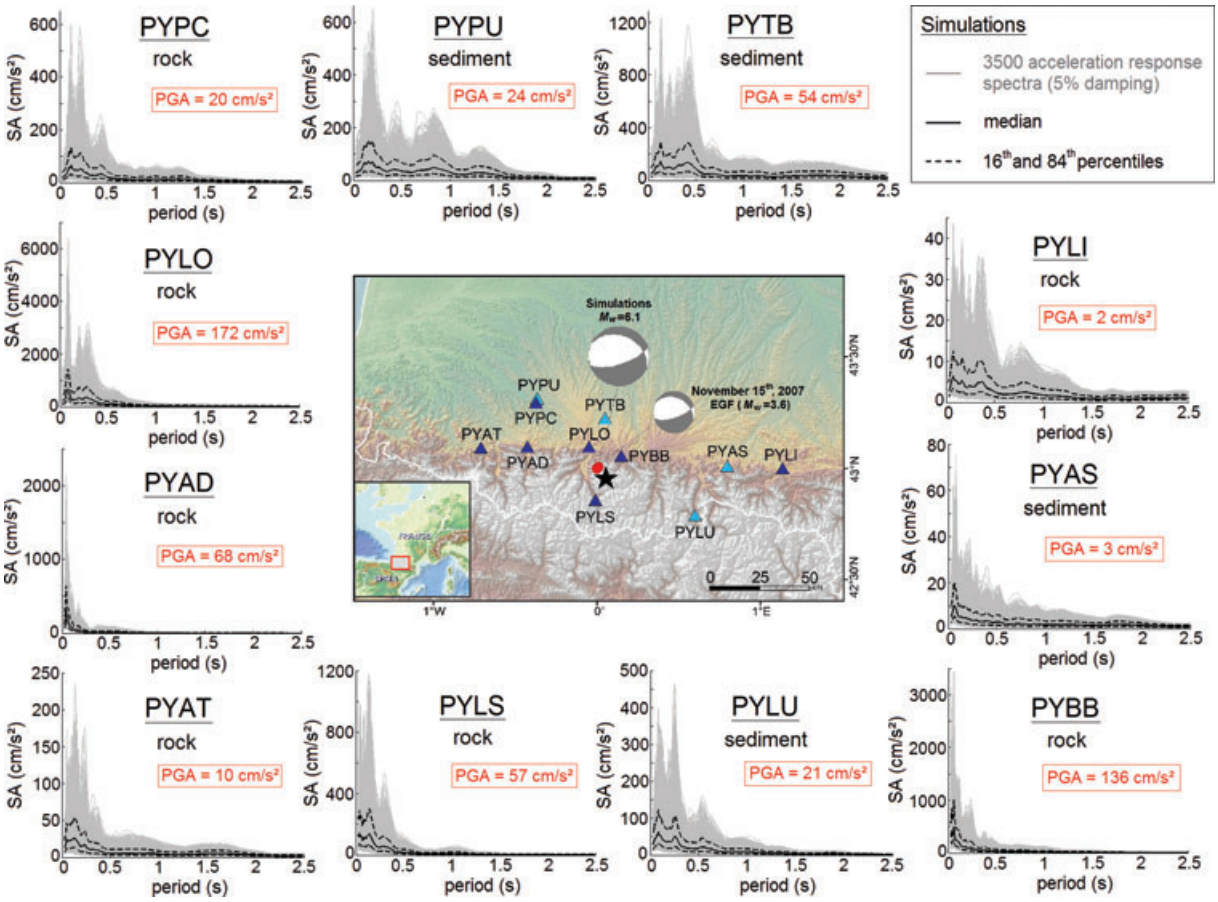

Figure 13. Simulation results in terms of acceleration response spectra (in grey) and median PGA (values in red) obtained for a $M_w = 6.1$ earthquake at each station (eastern component). Median and 84th–16th percentiles (in black) are computed from the overall spectral acceleration distribution including an uncertainty on the stress drop ratio parameter C.

Table 6. Ground motion prediction equations (GMPEs) used for the comparison with simulation results. Magnitude and distance definitions and their range of validity are given for each. M_J is Japanese Meteorological Agency magnitude, M_S is surface-wave magnitude, M_w is moment magnitude, R_{hypo} is hypocentral distance and R_{JB} is Joyner & Boore (1981) distance.

Authors	Area and time coverage of data set	Magnitude range of validity	Distance range of validity (km)	Horizontal component definition
Lussou *et al.* (2001)	Japan 1996–1998	$3.5 \leq M_J \leq 6.3$	$10 \leq R_{hypo} \leq 200$	Not specified
Berge-Thierry *et al.* (2003)	Europe (83 per cent) California (17 per cent) 1952–1997	$4.0 \leq M_S \leq 7.9$	$4 \leq R_{hypo} \leq 330$	Both horizontal components
Ambraseys *et al.* (2005)	Europe and Middle East 1973–2003	$M_w \geq 5.0$	$R_{JB} < 100$	Larger horizontal component

7 COMPARISON BETWEEN SIMULATION RESULTS AND MACROSEISMIC INTENSITIES OF THE 1660 EARTHQUAKE

This part of the study consists in comparing our acceleration predictions at the 11 stations with macroseismic intensities of the 1660 historical event (Fig. 15).

During the last decades, many studies have been conducted to establish correlation equations that relate instrumental ground motion parameters to observed intensity information (e.g. Murphy & O'Brien 1977; Trifunac & Brady 1975; Ambraseys 1974, for the oldest ones). These ground motion intensity conversion equations (GMICEs) are empirically derived from regression analysis of the database for which both ground motion records and nearby intensity observations are available. GMICEs are mostly developed for rapid damage assessment, like shake map applications. However, the availability of such empirical relationships also enables us to estimate possible ground motion parameter ranges of historical earthquakes. In our case, GMICEs provide us with the opportunity to make a direct link between our ground motion simulations and the intensities of the 1660 historical earthquake.

To transform our simulated PGA and PGV values into intensity values, we used three different PGA-Intensity and PGV-Intensity empirical relationships recently developed by Wald *et al.* (1999), Atkinson & Kaka (2007) and Tselentis & Danciu (2008). The data sets used to derive these GMICEs and their intensity ranges of

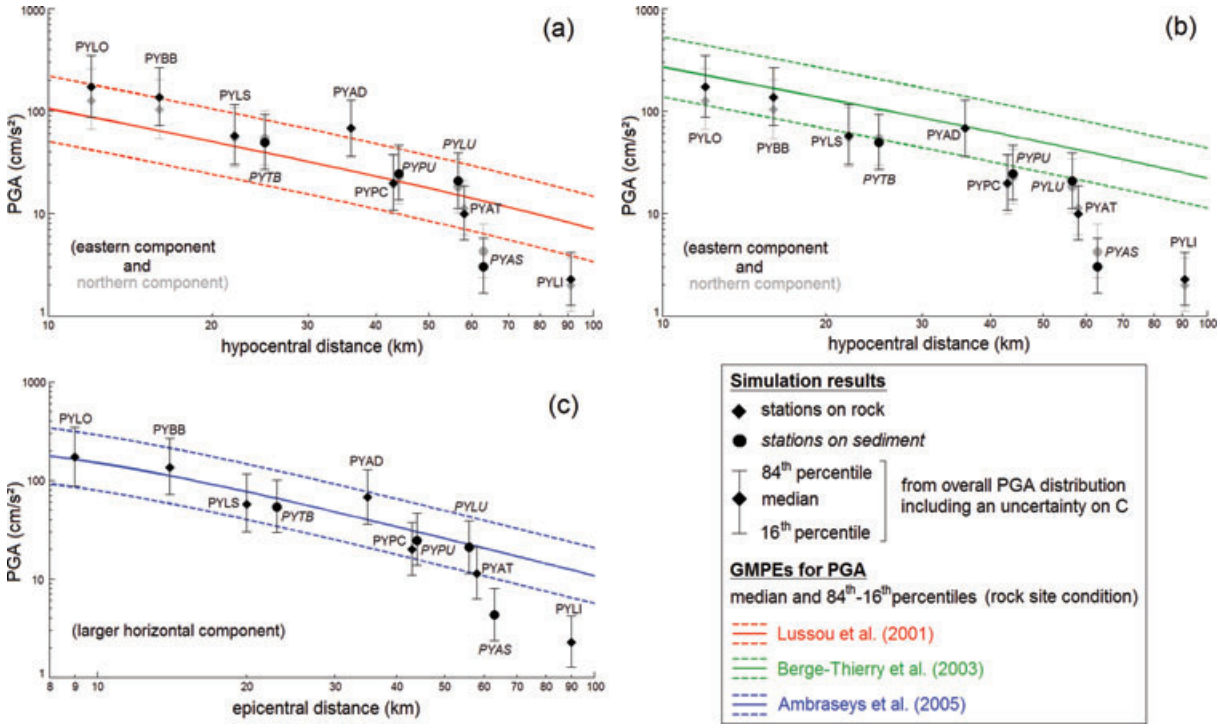

Figure 14. Peak Ground Accelerations obtained from simulation of the $M_w = 6.1$ earthquake at each station (both at rock and soil sites) as a function of source-to-site distance. Black and grey symbols are for the eastern and northern components, respectively. Median and 84th–16th percentiles are computed from overall PGA distribution including an uncertainty on the stress drop ratio parameter *C*. They are compared with PGA values predicted for rock site conditions by the ground motion prediction equations of (a) Lussou *et al.* (2001) on both horizontal components (black: east, grey: north); (b) Berge-Thierry *et al.* (2003) on both horizontal components (black: east, grey: north); (c) Ambraseys *et al.* (2005) for the larger horizontal component.

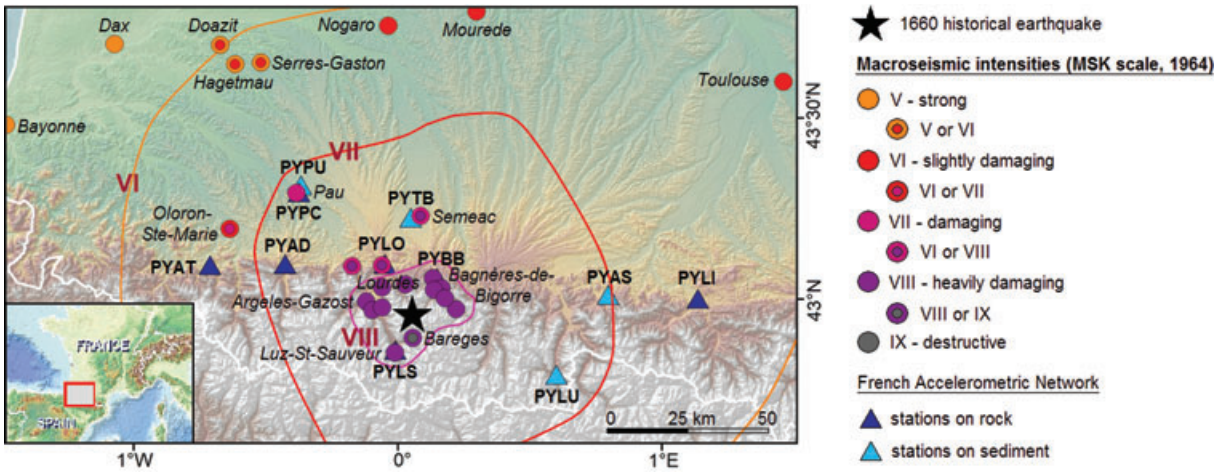

Figure 15. Macroseismic intensities (MSK scale, 1964) and isoseists for the 1660 June 21, historical earthquake. The macroseismic epicentre of the 1660 event is plotted as a black star with a location uncertainty of about 10 km. The intensity value assigned to each point was assessed from interpretation of available historical documents where felt shaking and damage was reported (SisFrance catalogue, BRGM *et al.* 2004).

validity are indicated in Table 7. Wald *et al.* (1999) empirical relationships are those usually used to produce shake maps in California. These PGA-Intensity and PGV-Intensity correlation equations are obtained from eight large Californian earthquakes. Atkinson & Kaka (2007) relationships were developed from small to moderate earthquakes both felt and recorded in the central United States region. This database was supplemented with data from larger events that occurred in California. The equations defined by Atkinson & Kaka (2007) take into account the influence of magnitude and distance, which is not the case for the equations of Wald *et al.* (1999). The empirical relationships developed by Tselentis & Danciu (2008) are based on data recorded in Greece and include effects of magnitude, distance and local soil conditions. Note that intensity values cannot be estimated from these equations with a precision better than one unit.

Using these three GMICEs, we computed an intensity level for each station from median values of PGA obtained from simulations. In Fig. 16, the intensity ranges obtained from ground motion simulations are compared with macroseismic intensities of the 1660 historical earthquake (SisFrance, BRGM *et al.* 2004). We note that

Table 7. Data sets used to derive ground motion intensity conversion equations (GMICEs), with their intensity range of validity and the horizontal component definition. M_w is moment magnitude and MMI is Modified Mercalli Intensity.

Authors	Data set	Intensity range of validity	Horizontal component definition
Tselentis & Danciu (2008)	Greece (1973–1999) $4 \leq M_w \leq 6.9$	IV ≤ MMI ≤ VIII	Both horizontal components
Wald *et al.* (1999)	California (1971–1994) $5.8 \leq M_w \leq 7.3$	V ≤ MMI ≤ VIII	Geometric mean
Atkinson & Kaka (2007)	Central United States (2000–2005) $1.8 \leq M_w \leq 4.6$ + California (2000–2004) $3.5 \leq M_w \leq 7.1$	II ≤ MMI ≤ IX	Both horizontal components

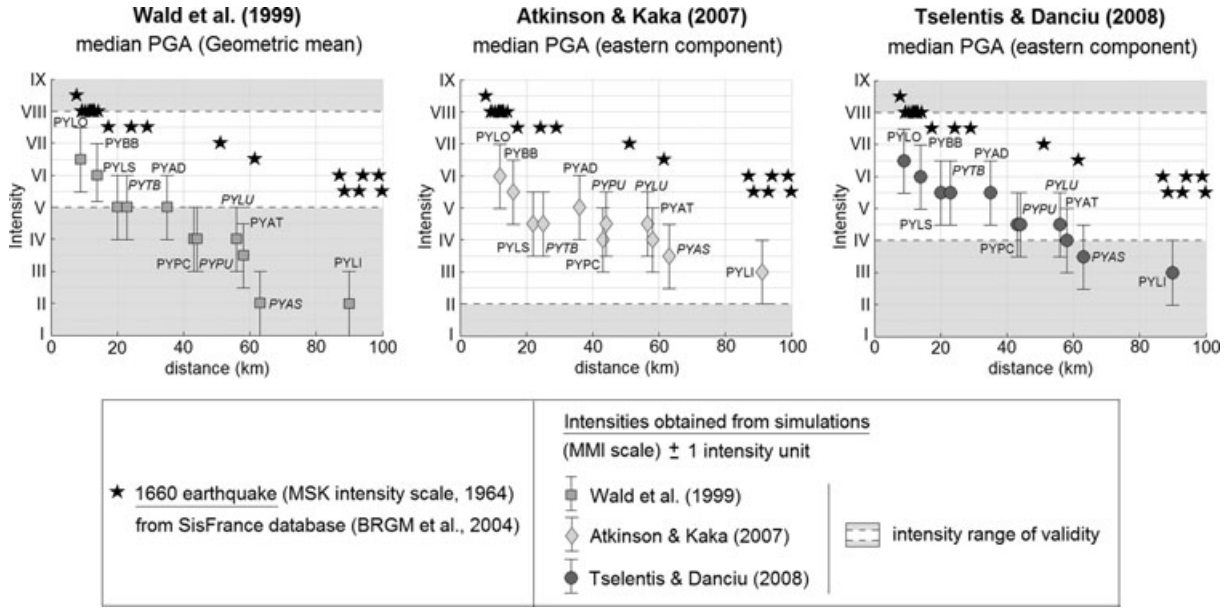

Figure 16. Comparison between macroseismic MSK intensities of the 1660 earthquake (SisFrance, BRGM *et al.* 2004) and intensity levels (MMI scale) expected at each station from the ground motion simulations of an $M_w = 6.1$ earthquake. For each station, median values of PGA of simulations (including an uncertainty on the stress drop ratio parameter) are transcribed into intensity values (± one intensity unit) by using PGA-Intensity empirical relationships of Wald *et al.* (1999), Atkinson & Kaka (2007) and Tselentis & Danciu (2008).

two different intensity scales are used: macroseismic intensities of the 1660 event are expressed in the MSK scale (Medvedev *et al.* 1964), whereas the results obtained from empirical relationships are expressed in the Modified Mercalli Intensity scale (Wood & Neumann 1931; see Musson *et al.* (2009) for a review of a large number of intensity scales). However, as shown by Barosh (1969), the two scales are essentially similar over their whole range of values. Fig. 16 clearly shows that intensity values obtained from PGA of simulations are too small compared with macroseismic intensities of the 1660 earthquake. For example, at a distance of about 10 km we obtained intensity values equal to VI or VI–VII from simulations, where the reported intensity is VIII, corresponding to major destruction (as reported in historical documents for the cities of Lourdes and Bagnères-de-Bigorre). From the 84th percentile values of PGA, intensity reach a maximal value of VII at a distance of 10 km. Similar results are obtained with the PGV, which is sometimes recognized as a better indicator of the destructive potential of ground motions than PGA (e.g. Wald *et al.* 1999; Boatwright *et al.* 2001; Kaka & Atkinson 2004). Moreover, even if the three different GMICEs used here are developed for different regions of the world, the results are in good agreement between themselves. Thus, on the whole, there is a difference of up to two intensity units between macroseismic intensities assessed for the 1660 earthquake and intensity levels predicted by empirical relationships from simulation results.

8 DISCUSSION: WAS THE 1660 EARTHQUAKE LARGER THAN $M_w = 6.1$?

In this section, we observed that intensity levels corresponding to our ground motion simulations of an $M_w = 6.1$ earthquake were clearly lower than macroseismic intensities of the 1660 historical earthquake. This result led us to discuss the origin of this discrepancy, in particular to question whether the 1660 event was larger than an $M_w = 6.1$ earthquake. To make a critical analysis of this hypothesis, the following points must be discussed:

8.1 Macroseismic information: epicentre and depth

Collecting historical information to establish macroseismic maps is not an easy task. For the 1660 event, the macroseismic epicentre appears rather well defined (within 10 km). However, if the 1660 event had a strong directivity, the macroseismic epicentre might be

shifted by several kilometres with respect to the real epicentre (e.g. Grandin *et al.* 2007, for the 1755 great Lisbon earthquake). Thus the location of the 1660 event may be somewhat different from that of the two recent small events.

No information is known about the depth of the 1660 event. The distance between isoseists is informative of this depth, thus depth may theoretically be retrieved from the macroseismic maps if an attenuation model is available (Levret *et al.* 1994). Although the depth is not given in the historical catalogues for this event, its isoseists are clearly those of a superficial event, similar to most of the Pyrenean events. Levret *et al.* (1994) show that 70 per cent of the focii of French historical events are in the depth range of 2.5–12.5 km. Instrumental seismicity also reveals that most of the earthquakes in the Lourdes region are between 5 and 13 km in depth (Rigo *et al.* 2005). It is thus realistic to ascribe to the 1660 event the same depth as that of the small event used as an EGF.

8.2 Macroseismic information: intensity–magnitude relationship

The macroseismic magnitude of the 1660 event ($M_l = 6.1 \pm 0.4$; Levret *et al.* 1996) was obtained by using the Levret *et al.* (1994) relationship between local magnitude, intensity and focal distance. This empirical relationship was established from 73 French earthquakes for which macroseismic data and instrumental magnitudes are both available.

Uncertainties accumulate at each step of historical data analysis. The determination of intensity from damage is partially subjective. Intensity values depend on site conditions, their values for a given magnitude and a given distance are thus very scattered. The uncertainty on focal depth should also have a small impact on the magnitude estimate: the magnitude would be underestimated if the focal depth is underestimated.

A more critical point is that the magnitude–intensity relationship is established with only two events with $M_l \geq 6$, and with a maximum intensity of VII. It is thus poorly constrained for large events. Moreover, a single relationship is established for the whole French home territory, whereas significant regional variations in attenuation have been observed (Drouet *et al.* 2010). The strong attenuation in the Pyrenees may result in an underestimation of the magnitudes from the standard intensity–magnitude relationship.

Finally, the magnitude determined by Levret *et al.* (1996) is a local magnitude M_l, whereas we use a moment magnitude M_w for simulating the ground motions. For moderate Pyrenean events, Drouet *et al.* (2005) found a difference of about 0.5 between these two magnitudes. It is also the case for the two small events used in this paper (the 2006 event, $M_l = 5.0$, $M_w = 4.5$, and the 2007 event, $M_l = 4.1$, $M_w = 3.6$). This magnitude difference, extrapolated to large events, predicts a moment magnitude of about $M_w = 5.6$ for the 1660 event. With such a low value, the agreement between our simulated ground motions and the macroseismic data would be worse. Note, however, that the moment magnitude proposed by Cara *et al.* (2008) for the 1660 event, $M_w = 6.1$, suggests that the difference between M_l and M_w cannot be extrapolated to large earthquakes.

8.3 Macroseismic information: ground motion values

The use of GMICEs to transcribe simulation results into intensity values is another source of difficulties. Macroseismic intensity represents, on a qualitative and discrete scale, a complex function between ground motions, damage levels and human perception of shaking. Response of the structures to shaking and human sensitivity are both frequency-dependent. On the other hand, each ground motion parameter (in particular PGA) concerns different characteristics and frequency content of the seismogram (Souriau 2006). A correlation equation between instrumental ground motion parameters and macroseismic intensity thus includes hidden parameters, such as frequency. The resistance of buildings, which has increased through centuries, is another difficulty in the comparison of the intensity data of the 1660 event with equations derived from recent intensity measurements. The punctual intensity values obtained from the simulation were not obtained at the same points as those used to derive the intensity map, which is an additional source of uncertainty. Moreover, most of our accelerometric measurements are at rock site conditions, whereas macroseismic intensity values mostly come from the cities and villages, which are built in the sedimentary basins. Thus, when used to predict intensity levels from simulation results, GMICEs should thus be considered in a critical way.

8.4 Shortcomings of the simulation method

Assuming the magnitude $M_w = 6.1$ ascribed to the 1660 earthquake is correct, some shortcomings of the EGF simulation method should be pointed out to explain differences between simulation results and intensity data of the 1660 event.

For the computation of ground motion simulations, we have assumed that location, focal depth and focal mechanisms are the same for the 1660 event and for the small earthquake used as an EGF. This dependence on the EGF characteristics is not a shortcoming of the method in itself. However, a different fault mechanism or depth for the 1660 event cannot be excluded. It would perturb the results in a way, which is unfortunately difficult to quantify.

The EGF method does not account for nonlinear soil behaviour. This point is certainly not crucial to our study because the levels of acceleration found are rather low and should not induce non-linear effects.

This simulation method is based on a point-source representation of the fault, thus it does not allow us to take precisely into account a specific directivity effect of the rupture. Nothing is known about the rupture of the 1660 event. Therefore, to substitute for the directivity effect, we ran different simulations for which the stress drop parameter C was set at different values corresponding to rupture durations from 3.6 to 7.6 s for the target event. The good fit of the GPMEs suggests our simulations are correct; however, the underprediction of the intensities led us to wonder whether the ground motion variability produced by our simulations is large enough.

In summary, interpretation of the macroseismic data of the 1660 earthquake is far from simple. It is possibly affected by location, magnitude, and by the difficulty to convert intensity data into ground motion values. Furthermore, the simulation method might have underestimated the radiation of the 1660 event because of the impossibility to account for the details of the rupture. All of these reasons lead us to speculate whether the 1660 event could have a M_w magnitude larger than 6.1, but we cannot give a definite conclusion in this respect. Alternatively, macroseismic intensities may have been overestimated due to the poor quality of the constructions and to their locations on sediment.

9 CONCLUSION

Using the opportunity provided by two moderate earthquakes ($M_w = 3.6$ and $M_w = 4.5$), well recorded by an accelerometric

network in the Pyrenees, we simulated seismograms of a larger event similar to the 1660 historical earthquake, that caused severe damage and casualties. We first validated the approach by simulating the $M_w = 4.5$ event using the $M_w = 3.6$ event as an EGF. Data analysis revealed a clear directivity effect of the rupture process of the $M_w = 4.5$ event which, once taken into account, led to a very good agreement between observations and simulations. The directivity effect was formally taken into account by means of a 'station-dependent' stress drop ratio parameter. In this example, we observed that directivity effect has an influence on ground motion levels comparable to that of site effects.

Using the $M_w = 3.6$ event, which does not exhibit directivity in its rupture, we then simulated the 1660 historical event for which a magnitude of $M_w = 6.1$ has been proposed. This simulation allowed us to generate realistic seismograms and to estimate the PGA in the main cities where destruction was reported. One of the important results is the good agreement between simulated PGA values and the predictions of empirical ground motion equations for an $M_w = 6.1$ event. Our simulation results were then converted into macroseismic intensity using three published empirical GMICEs. We found that our values were always lower than the macroseismic intensities collected. This inconsistency led us to discuss whether the 1660 event had a magnitude larger than $M_w = 6.1$, or alternately to question the validity of the conversion from intensities to magnitudes.

The approach we have developed nevertheless appears very promising for simulating the ground motion of a large earthquake, when only the records of small earthquakes are available. This gives an interesting complement to the intensity map for anticipating damage in the case of large events, for defining seismic zoning and for specifying seismic building codes in a region.

ACKNOWLEDGMENTS

We thank the persons in charge of the seismological and accelerometric networks in the French Pyrenees, particularly Mathieu Sylvander and Marie Calvet at the Observatoire Midi-Pyrénées, and Pascal Dominique at the Bureau de Recherches Géologiques et Minières. We also thank the staff of the RAP (Réseau Accélérométrique Permanent Français), which provides open, high quality data. We thank David Baumont from the Institut de Radioprotection et de Sureté Nucléaire and Michel Cara from the Bureau Central de Sismologie Français, for fruitful discussions. We also thank M. Cocco, J. Zaradnick and an anonymous reviewer for their remarks and questions that helped to improved the manuscript. Financial support for the grant thesis has been provided by the French Ministry of Environment through the Groupement d'Interêt Scientifique GIS-RAP, and by the French Ministry of Enseignement Supérieur et Recherche.

REFERENCES

Aki, K., 1967. Scaling law of seismic spectrum, *J. geophys. Res.,* **72,** 1217–1231.

Alasset, P-J. & Meghraoui, M., 2005. Active faulting in the western Pyrénées (France): paleoseismic evidence for late Holocene ruptures, *Tectonophysics,* **409,** 39–54.

Allmann, B.P. & Shearer, P.M., 2009. Global variations of stress drop for moderate to large earthquakes, *J. geophys. Res.,* **114,** B01310, doi:10.1029/2008JB005821.

Ambraseys, N., 1974. The correlation of intensity with ground motions, in *Proceedings of the 14th Conf. of the European Seismological Commission,* Trieste, Italy.

Ambraseys, N., Simpson, K.A. & Bommer, J.J., 1996. Prediction of horizontal response spectra in Europe, *Int. J. Earthq. Eng. Struct. Dyn.,* **25,** 371–400.

Ambraseys, N.N., Douglas, J., Sarma, S.K. & Smit, P.M., 2005. Equations for the estimation of strong ground motions from shallow crustal earthquakes using data from Europe and the Middle-East: horizontal peak ground acceleration and spectral acceleration, *Bull. seism. Soc. Am.,* **3,** 1–53, doi:10.1007/s10518-005-0183-0.

Atkinson, G.M. & Kaka, S.I., 2007. Relationships between felt intensity and instrumental ground motion in the central United States and California, *Bull. seism. Soc. Am.,* **97,** 497–510.

Barosh, P.K., 1969. Use of seismic intensity data to predict the effects of earthquakes and underground nuclear explosions in various geological settings, *US Geol. Surv. Bull.,* 1279, Washington D.C., 93pp.

Beauval, C., Honoré, L. & Courboulex, F., 2009. Ground-motion variability and implementation of a probabilistic-deterministic hazard method, *Bull. seism. Soc. Am.,* **99,** 2992–3002, doi:10.1785/0120080183.

Beeler, N.M., Wong, T.F. & Hickman, S.H., 2003. On the expected relationships between apparent stress, static stress drop, effective shear fracture energy and seismic efficiency, *Bull. seism. Soc. Am.,* **93,** 1381–1389.

Berge-Thierry, C., Cotton, F., Scotti, O., Griot-Pommera, D.A. & Fukushima, Y., 2003. New empirical response spectral attenuation laws for moderate European earthquakes, *J. Earthq. Eng.,* **7,** 193–222.

Bernard, P., Czitrom, G., Dubié, J-Y., Godefroy, P., Lambert, J. & Levret-Albaret, A., 1997. *Les tremblements de Terre en France*, ed. Lambert J., Editions BRGM, Orléans, 196pp.

Boatwright, J., 2007. The persistence of directivity in small earthquakes, *Bull. seism. Soc. Am.,* **97,** 1850–1861.

Boatwright, J., Thywissen, K. & Seekins, L., 2001. Correlation of ground motion and intensity for the 17 January 1994 Northridge, California, earthquake, *Bull. seism. Soc. Am.,* **91,** 739–752.

Bragato, L. & Slejko, D., 2005. Empirical ground-motion attenuation relations for the eastern Alps in the magnitude range 2.5–6.3, *Bull. seism. Soc. Am.,* **95,** 252–276.

BRGM-IRSN-EDF *et al.*, 2004. Histoire et caractéristiques des séismes ressentis en France métropolitaine et sur ses abords, SisFrance catalog. Available at: http://www.sisfrance.net/ (last access 2010 September).

Brune, J.N., 1970. Tectonic stress and the spectra of seismic shear waves from earthquakes, *J. geophys. Res.,* **75,** 4997–5009.

Cara, M., Alasset, P.-J. & Sira, C., 2008. Magnitude of historical earthquakes, from macroseismic data to seismic waveform modelling: application to the Pyrenees and a 1905 earthquake in the Alps, *Historical Seismol.,* **2,** 369–384, doi:10.1007/978-1-4020-8222-1_18.

Choukroune, P., 1992. Tectonic evolution of the Pyrenees, *Annu. Rev. Earth planet. Sci.,* **20,** 143–158.

Cotton, F., Pousse, G., Bonilla, F. & Scherbaum, F., 2008. On the discrepancy of recent European ground-motion observations and predictions from empirical models: analysis of Kik-net accelerometric data and point-sources stochastic simulations, *Bull. seism. Soc. Am.,* **98,** 2244–2261, doi:10.1785/0120060084.

Courboulex, F., Converset, J., Balestra, J. & Delouis, B., 2010. Ground-motion simulations of the 2004 Mw 6.4 Les Saintes, Guadeloupe, earthquake using ten smaller events, *Bull. seism. Soc. Am.,* **100,** 116–130, doi:10.1785/0120080372.

Deichmann, N., 2006. Local magnitude, a moment revisited, *Bull. seism. Soc. Am.,* **96,** 1267–1277, doi:10.1785/0120050115.

Douglas, J., 2003. Earthquake ground motion estimation using strong-motion records: a review of equations for the estimation of peak ground acceleration and response spectral ordinates, *Earth Sci. Rev.,* **61,** 43–104.

Drouet, S., Souriau, A. & Cotton, F., 2005. Attenuation, seismic moments, and site effects for weak-motion events: application to the Pyrenees, *Bull. seism. Soc. Am.,* **95,** 1731–1748, doi:10.1785/0120040105.

Drouet, S., Scherbaum, F., Cotton, F. & Souriau, A., 2007. Selection and ranking of ground motion models for seismic hazard analysis in the Pyrenees, *J. Seism.,* **11,** 87–100, doi:10.1007/s10950-006-9039-6.

Drouet, S., Cotton, F. & Guéguen, P., 2010. v_{S30}, k, regional attenuation and M_w from accelerograms: application to magnitude 3–5 French earthquakes, *Geophys. J. Int.,* **182,** 880–898, doi:10.1111/j.1365-246X.2010.04626.x.

Dubos, N., Sylvander, M., Souriau, A., Ponsolles, C., Chevrot, S., Fels, J-F. & Benahmed, S., 2004. Analysis of the 2002 May earthquake sequence in the central Pyrenees, consequences for the evaluation of the seismic risk at Lourdes, France, *Geophys. J. Int.,* **156,** 527–540, doi:10.1111/j.1365-246X.2004.02091.x.

Gagnepain, J., Modiano, T., Cisternas, A., Ruegg, J.C., Vadell, M., Hatzfeld, D. & Mezcua, J., 1980. Sismicité de la région d'Arette (Pyrénées Atlantiques) et mécanismes au foyer, *Ann. Geophys.,* **36,** 499–508.

Gagnepain-Beyneix, J., Haessler, H. & Modiano, T., 1982. The Pyrenean earthquake of February 29 1980, an example of complex faulting, *Tectonophysics,* **85,** 273–290.

Grandin, R., Borges, J.F., Bezzegoud, M., Caldeira, B. & Carrilho, F., 2007. Simulations of strong ground motion in SW Iberia for the 1969 February 28 (Ms = 8.0) and the 1755 November 1 (M∼8.5) earthquakes – II. Strong ground motion simulations, *Geophys. J. Int.,* **171,** 807–822.

Hartzell, S.H., 1978. Earthquake aftershocks as Green's functions, *Geophys. Res. Lett.,* **5,** 1–4.

Heaton, T.H., Tajima, F. & Mori, A.W., 1986. Estimating ground motions using recorded accelerograms, *Surv. Geophys.,* **8,** 25–83.

Houston, H., 2001. Influence of depth, focal mechanism, and tectonic setting on the shape and duration of earthquake source time functions, *J. geophys. Res.,* **106,** 11 137–11 150.

Ide, S. & Beroza, G.C., 2001. Does apparent stress vary with earthquake size? *Geophys. Res. Lett.,* **28,** 3349–3352.

Irikura, K. & Kamae, K., 1994. Estimation of strong ground motion in broad-frequency band based on a seismic source scaling model and an empirical Green's function technique, *Annali di Geofisica,* **XXXVII,** 1721–1743.

Joyner, W.B. & Boore, D.M., 1981. Peak horizontal acceleration and velocity from strong-motion records including records from the 1979 Imperial Valley, California, earthquake, *Bull. seism. Soc. Am.,* **71,** 2011–1038.

Joyner, W.B. & Boore, D.M., 1986. On simulating large earthquakes by Green's function addition of smaller earthquakes, in *Earthquake Source Mechanics,* Vol. 37, Maurice Ewing Series 6, pp. 269–274, eds Das, S., Boatwright, J. & Scholtz, C.H., American Geophysical Union, Washington, D.C.

Kaka, S.I. & Atkinson, G.M., 2004. Relationships between instrumental ground-motion parameters and modified Mercalli intensity in eastern North America, *Bull. seism. Soc. Am.,* **94,** 1728–1736.

Kanamori, H. & Rivera, L., 2004. Static and dynamic scaling relations for earthquakes and their implications for rupture speed and stress drop, *Bull. seism. Soc. Am.,* **94,** 314–319.

Kohrs-Sansorny, C., Courboulex, F., Bour, M. & Deschamps, A., 2005. A two-stage method for ground-motion simulation using stochastic summation of small earthquakes, *Bull. seism. Soc. Am.,* **95,** 1387–1400.

Lambert, J. & Levret-Albaret, A., 1996. Mille ans de séismes en France, *Ouest Editions,* Nantes, 78pp.

Levret, A., Backe, J.C. & Cushing, M., 1994. Atlas of macroseismic maps for French earthquakes with their principal characteristics, *Nat. Haz.,* **10,** 19–46.

Levret, A., Cushing, M. & Peyridieu, G., 1996. Recherche des caractéristiques de séismes historiques en France. Atlas de 140 cartes macrosismiques, IPSN, Paris, France (2 vol.).

Lussou, P., Fukushima, Y., Bard, P.Y. & Cotton, F., 2001. Seismic design regulation codes: contribution of Knet data to site effect evaluation, *J. Earthq. Eng.,* **5,** 13–33.

Marin, S., Avouac, J-P, Nicolas, M. & Schlupp, A., 2004. A probabilistic approach to seismic hazard in metropolitan France, *Bull. seism. Soc. Am.,* **94,** 2137–2163.

Medvedev, S., Sponheuer, W. & Karnik, V., 1964. Neue seismische Skala Intensity scale of earthquakes, 7.Tagung der Europäischen Seismologischen Kommission vom 24.9. bis 30.9.1962. *Jena, Veröff. Institut für Bodendynamik und Erdbebenforschung in Jena*, Vol. 77, pp. 69–76. Deutsche Akademie der Wissenschaften zu Berlin.

Murphy, J.R. & O'Brien, L.J., 1977. The correlation of peak ground acceleration amplitude with seismic intensity and other physical parameters, *Bull. seism. Soc. Am.,* **67,** 877–915.

Musson, R.M.W., Grünthal, G. & Stucchi, M., 2009. The comparison of macroseismic intensity scales, *J. Seism.,* **14,** 413–428, doi:10.1007/s10950-009-9172-0.

Nocquet, J.-M. & Calais, E., 2004. Geodetic measurements of crustal deformation in the Western Mediterranean and Europe, *Pure appl. Geophys.,* **161,** 661–681.

Olivet, J.L., 1996. La cinématique de la plaque Ibérique (Kinematics of the Iberian Plate), *Bull. Centres Rech. Explor.-Prod. Elf Aquitaine,* **20,** 131–195.

Ordaz, M., Arboleda, J. & Singh, S.K., 1995. A scheme of random summation of an empirical Green's function to estimate ground motions from future large earthquakes, *Bull. seism. Soc. Am.,* **85,** 1635–1647.

Pequegnat, C., Guéguen, P., Hatzfeld, D. & Langlais, M., 2008. The French Accelerometric Network (RAP) and National Data Center (RAP-NDC), *Seismol. Res. Lett.,* **79,** 79–89.

Reiter, L., 1990. *Earthquake Hazard Analysis: Issues and Insights,* Columbia University Press, New York, NY, 254pp.

Rigo, A., Souriau, A., Pauchet, H., Grésillaud, A., Nicolas, M., Olivera, C. & Figueras, S., 1997. The February 1996 earthquake sequence in the eastern Pyrenees: first results, *J. Seism.,* **1,** 3–14, doi:10.1023/A:1009711512921.

Rigo, A., Souriau, A., Dubos, N., Sylvander, M. & Ponsolles, C., 2005. Analysis of the seismicity in the central part of the Pyrenees (France), and tectonic implications, *J. Seism.,* **9,** 211–222.

Ruiz, M., Gallart, J., Diaz, J., Olivera, C., Pedreira, D., Lopez, C., Gonzalez-Cortina, J.M. & Pulgar, J.A., 2006. Seismic activity at the western Pyrenean edge, *Tectonophysics,* **412,** 217–235, doi:10.1016/j.tecto.2005.10.034.

Salichon, J., Kohrs-Sansorny, C., Bertrand, E. & Courboulex, F., 2010. A Mw 6.3 earthquake scenario in the city of Nice (southeast France): ground motion simulations, *J. Seism.,* **14,** 523–541, doi:10.1007/s10950-009-9180-0.

Scherbaum, F., Cotton, F. & Smit, P., 2004. On the use of response spectral reference data for the selection and ranking of ground-motion models for seismic hazard analysis in regions of moderate seismicity: the case of rock motion, *Bull. seism. Soc. Am.,* **94,** 1–22.

Secanell, R. *et al*., 2008. Probabilistic seismic hazard assessment of the Pyrenean region, *J. Seism.,* **12,** 323–341, doi:10.1007/s10950-008-9094-2.

Souriau, A., 2006. Quantifying felt events: a joint analysis of intensities, accelerations and dominant frequencies, *J. Seism.,* 10, doi:10.1007/s10950-006-2843-1.

Souriau, A. & Pauchet, H., 1998. A new synthesis of Pyrenean seismicity and its tectonic implications, *Tectonophysics,* **290,** 221–244.

Sylvander, M., Souriau, A., Rigo, A., Tocheport, A., Toutain, J-P., Ponsolles, C. & Benahmed, S., 2008. The 2006 November, Ml = 5.0 earthquake near Lourdes (France): new evidence for NS extension across the Pyrenees, *Geophys. J. Int.,* **175,** 649–664, doi:10.1111/j.1365-246X.2008.03911.x.

Trifunac, M.D. & Brady, A.G., 1975. On the correlation of seismic intensity with peaks of recorded ground motion, *Bull. seism. Soc. Am.,* **65,** 139–162.

Tselentis, G-A. & Danciu, L., 2008. Empirical relationships between modified mercalli intensity and engineering ground-motion parameters in Greece, *Bull. seism. Soc. Am.,* **98,** 1863–1875, doi:10.1785/0120070172.

Vogt, J., 1979. Les tremblements de terre en France, *Mem. BRGM,* 96, Orleans, France, 220pp.

Wald, D.J., Quitoriano, V., Heaton, T.H. & Kanamori, H., 1999. Relationships between peak ground acceleration, peak ground velocity, and modified Mercalli intensity in California, *Earthq. Spectra,* **15,** 557–564.

Wennerberg, L., 1990. Stochastic summation of empirical Green's functions, *Bull. seism. Soc. Am.,* **80,** 1418–1432.

Wood, H.O. & Neumann, F., 1931. Modified Mercalli Intensity scale of 1931, *Bull. seism. Soc. Am.,* **21,** 277–283.